# Morphological Changes Induced by TKS4 Deficiency Can Be Reversed by EZH2 Inhibition

Mevan Jacksi , Eva Schad , Agnes Tantos *

Posted Date: 13 March 2024

doi: 10.20944/preprints202403.0787.v1

Keywords: EZH2; Enhancer of zeste homolog 2; TKS4; signal transduction; long non-coding RNA; migration; invasion; EMT; epithelial-mesenchymal transition; Frank-Ter Haar syndrome

*Article*

# Morphological Changes Induced by TKS4 Deficiency Can Be Reversed by EZH2 Inhibition

**Mevan Jacksi [1,2,3], Eva Schad [1] and Agnes Tantos [1,*]**

[1] HUN-REN Research Centre for Natural Sciences, Budapest, Hungary; mehvan.jacksi@uoz.edu.krd (M.J.); schad.eva@ttk.hu (E.S.)
[2] Doctoral School of Biology, Institute of Biology, ELTE Eötvös Loránd University, Budapest, Hungary
[3] Department of Biology, College of Science, University of Zakho, Duhok, Iraq
* Correspondence: tantos.agnes@ttk.hu or agnes.tantos@ttk.hu

**Abstract: Background:** The scaffold protein tyrosine kinase substrate 4 (TKS4) undergoes tyrosine phosphorylation by the epidermal growth factor receptor (EGFR) pathway via Src kinase. The TKS4 deficiency in humans is responsible for the manifestation of a genetic disorder known as Frank-Ter Haar syndrome (FTHS). Based on our earlier investigation, the absence of TKS4 triggers migration, invasion, and epithelial-mesenchymal transition (EMT)-like phenomena while concurrently suppressing cell proliferation in HCT116 colorectal carcinoma cells. This indicates that TKS4 may play a unique role in the progression of cancer. In this study, we demonstrated that the enhancer of zeste homolog 2 (EZH2) and the histone methyltransferase of polycomb repressive complex 2 (PRC2) are involved in the migration, invasion, and EMT-like changes in TKS4-deficient cells (KO). EZH2 is responsible for the maintenance of the trimethylated lysine 27 on histone H3 (H3K27me3). **Methods:** We performed the transcriptome sequencing, chromatin immunoprecipitation, protein and RNA quantitative studies, cell mobility, invasion, and proliferation studies combined with/without EZH2 activity inhibitor 3-deazanoplanocine (DZNep). **Results:** We detected an elevation of global H3K27me3 levels in the TKS4 KO cells, which could be reduced with treatment with DZNep, an EZH2 inhibitor. Inhibition of EZH2 activity reversed the phenotypic effects of the knockout of TKS4, reducing the migration speed and wound healing capacity of the cells as well as decreasing the invasion capacity, while the decrease in cell proliferation became stronger. In addition, inhibition of EZH2 activity also reversed most epithelial and mesenchymal markers. We investigated the wider impact of TKS4 deletion on the gene expression profile of colorectal cancer cells using transcriptome sequencing of wild-type and TKS4 knockout cells, particularly before and after treatment with DZNep. Additionally, we observed changes in the expression of several protein-coding genes and long non-coding RNAs that showed a recovery in expression levels following EZH2 inhibition. **Conclusions:** Our results indicate that the removal of TKS4 causes a notable disruption in the gene expression pattern, leading to the disruption of several signal transduction pathways. Inhibiting the activity of EZH2 can restore most of these transcriptomics and phenotypic effects.

**Keywords:** EZH2; enhancer of zeste homolog 2; TKS4; signal transduction; long non-coding RNA; migration; invasion; EMT; epithelial-mesenchymal transition; Frank-Ter Haar syndrome

## 1. Introduction

Scaffold proteins govern cellular signaling by engaging in interactions and bringing various pathway components into close proximity, including enzymes and regulatory proteins [1]. The scaffold protein TKS4, encoded by the SH3PXD2B gene (gene ID: 285590), is a member of the p47 organizer protein family that contains four Src homology 3 domains (SH3) and a phox homology domain (PXD) [2]. TKS4 is associated with Src substrate adaptor proteins, which are essential for the production of podosomes and the invasion and growth of cancer cells [2,3]. TKS4 deletion or

 doi:10.20944/preprints202403.0787.v1



mutation in humans results in the appearance of a hereditary disorder known as FTHS [4–6], which is characterized by abnormal growth, skeletal abnormalities, and changes in facial features such as a large cornea, a flattened back of the head, a large cheek, and a small chin [7]. Similar phenotypic changes could be induced by the knockout of TKS4 in mice in an FTHS model. The TKS4-deficient mice show aberrant development resulting in stunted growth, craniofacial and skeletal deformities, glaucoma, hearing impairment, and a virtual lack of white adipose tissue [8]. TKS4 can regulate EMT-like processes through a mechanism not yet clearly defined [9,10]. Modifications in the differentiation of cell lineages and the maturation of cells were observed upon TKS4 depletion that can be connected to the development of FTHS [11]. The protein is mostly situated in the cytoplasm of inactive cells, but it relocates and binds to the membrane when exposed to epidermal growth factor (EGF) stimulation. This relocation is likely mediated by the Src kinase, which acts as a connector between TKS4 and EGFR [5]. EGFR is autophosphorylated upon EGF stimulation, which causes Src tyrosine phosphorylation. Then TKS4 binds to the SH3 domain of Src through its proline-rich motif. The kinase domain of Src phosphorylates tyrosine 25 of TKS4's PX domain, tyrosine 373 of its 3rd SH3 domain, and tyrosine 508 of its disordered region. The extended interaction between TKS4 and Src enhances the stability of the kinase and enables further substrate phosphorylation [12]. In summary, existing evidence indicates that TKS4 plays a central organizing role in several signal transduction pathways, and its presence is necessary for proper development and cellular function. However, the details of the molecular mechanisms of the protein's diverse effects are not fully understood yet.

The Polycomb Group (PcG) proteins, particularly PRC1 and PRC2, are widely recognized as mediating developmental gene silencing [7,13]. PRC1 and PRC2 have the ability to control the genomic structure and repress gene expression during the developmental process [14]. Genomic domains are classified into two categories: active domains and repressive domains. Both types regulate gene expression and determine the specific characteristics of a cell. The active domains comprise the genes involved in cell self-renewal, which are guided by super-enhancers, whereas the repressed domains include the genes marking the repressed lineage [15]. Furthermore, it has been shown that intact PcG domains are necessary for preserving the chromatin interaction landscape. Nevertheless, the precise mechanisms governing the formation of PcG domains and the complete understanding of PcG protein recruitment remain elusive, making the investigation of silencers more challenging [16–18].

Enhancer of zeste homolog 2 (EZH2) is a histone lysine methyltransferase responsible for the activity of PRC2, maintaining the trimethylated lysine 27 mark on histone H3 (H3K27me3) [19]. H3K27 trimethylation can be catalyzed to a lesser extent by Enhancer of Zeste Homolog 1 (EZH1) too [20]. H3K27me3 marks are associated with the regulation of genes specific to particular cell types. H3K27me3 is a known feature of silencers [17,21,22]. As a central factor in gene expression regulation, EZH2 is well-known for its involvement in EMT [23–25] and in several different signaling pathways [26,27]. It's overactivation is observed in several cancers [28,29] and higher EZH2 activity is generally accompanied by a worse disease prognosis and a more aggressive phenotype. Because of its recognized roles in cancer progression, regulating EZH2 activity is considered an important anti-tumour therapeutic method [30–32]. Since TKS4 is not directly involved in gene expression regulation, the previous observations regarding the induction of EMT-like processes [9] and the dysregulation of a wide variety of signaling pathways upon the deletion of TKS4 [33] raise the possibility of an indirect mediator that conveys the removal of TKS4 into altered gene expression patterns. Based on the overlaps between the roles of EZH2 and the observed changes in the TKS4 KO cells, we hypothesized that this mediator may be EZH2 itself. Therefore, in this work, we investigated the role of EZH2 in the cellular effects of TKS4 deletion with the aim of better understanding the molecular networks relying on TKS4.

 doi:10.20944/preprints202403.0787.v1



## 2. Materials and Methods

### *2.1. Cell Culture and TKS4 Knockout*

The TKS4 KO HCT116 cell line was created in accordance with the instructions provided in a 2019 publication [9]. HCT116 cells were grown in McCoy's 5A medium (Life Technologies, Paisley, UK) supplemented with 10% fetal bovine serum (FBS, Life Technologies, Paisley, UK) and 1% penicillin/streptomycin (Life Technologies, Paisley, UK). All cells were grown at 37 °C in a humidified atmosphere with 5% CO2. The TC20 Automated Cell Counter (Bio-Rad, Hercules, CA, USA) was used to measure the number and viability of cells using 0.4 percent trypan blue dye exclusion. An examination of the morphology was conducted utilizing an Axiovert 25 inverted microscope (Carl Zeiss Microscopy, Jena, Germany). Cell Line Authentication performed by Eurofins Genomics Europe Shared Services GmbH (85560 Ebersberg, Germany) confirmed the 100 % authenticity of the cells.

### *2.2. EZH2 Inhibitor Treatment*

3-deazanoplanocin A (DZNep) (Chem-Cruz, sc-351856) is an effective S-adenosylhomocysteine hydrolase inhibitor, which is a small molecule inhibitor of EZH2 activity. A cell viability assay and western blotting were conducted to determine the optimal concentration of DZNep for its impact on cell viability and determine the proper concentration (Supplementary Figure S1D). A concentration of 1 μM of DZNep had enough EZH2 inhibition activity (Figure 1.A) to lower dead cells; therefore, 1 μM was selected for the downstream experiments. HCT116 cells were cultured untreated or treated with DZNep for 48 hours in a 37 °C, 5% CO2 humidified incubator before being harvested for downstream investigations.

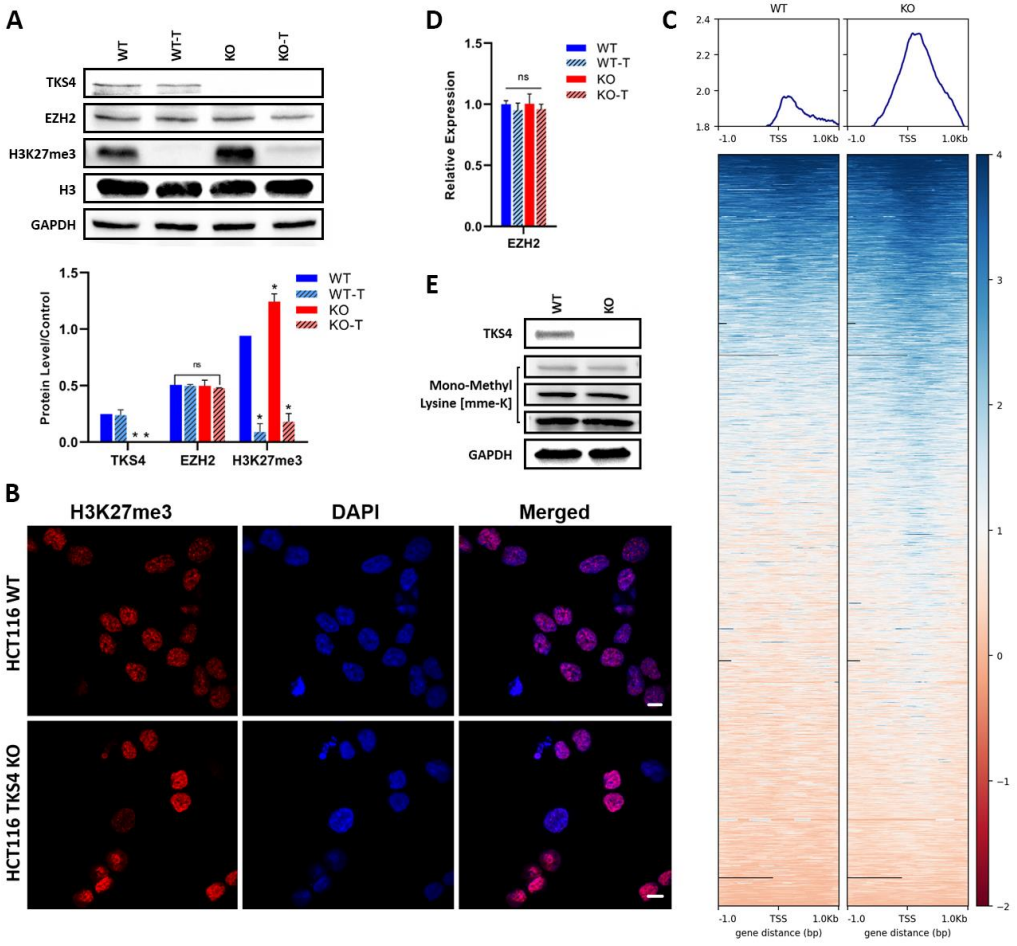


**Figure 1.** The effect of TKS4 deletion on H3K27me3. (**a**) Top: Western blot images of TKS4 and EZH2 H3K27me3. Histone 3 (H3) and beta-actin (ACTB) were used as protein loading controls. Bottom:

 doi:10.20944/preprints202403.0787.v1



analysis of western blotting images (n = 3). (**b**) Immunocytochemistry images showing the H3K27me3 levels in WT and TKS4 KO HCT116 cells. Nuclei were stained with DAPI. (**c**) Heatmap visualization of the H3K27me3 ChIP-seq data (RPGC Normalized). Heatmaps are sorted by ChIP-seq signal in descending order. EZH2 RNA expression levels (**d**) and global monomethylation levels (**e**) in the different cell lines and treatments. Scale bar: 20 μm Unmodified (WT), EZH2 activity inhibitor treated (WT-T), TKS4-deficient (KO), and TKS4-deficient treated with EZH2 activity inhibitor (KO-T) HCT116 cells. Results significant at $p > 0.005$ are marked with an asterisk. Original western blot images are presented on Supplementary Figure S1A.

### *2.3. Total RNA Extraction and Real-Time Quantitative PCR*

To lyse and isolate the total RNA of HCT116 cell lines, TRIzolTM Reagent (Life Technologies, Carlsbad, CA, USA) and the Direct-zol® MiniPrep kit (Zymo Research, Irvine, CA, USA) were used. DNA contamination is eliminated following a 15-minute DNAse I (Zymo Research, Irvine, CA, USA) treatment. The quality and quantity of the RNAs were determined using the nanophotometer IMPLEN (iBiotech, Czeck). Complementary DNA (cDNA) was synthesized from 1 μg of total RNA using the First Strand cDNA Synthesis Kit for RT-PCR (AMV) (Roche, Basel, Switzerland) and SuperScript™ III Reverse Transcriptase (Life Technologies, Paisley, UK). The real-time PCR experiments were carried out using TaqMan™ Fast Advanced Master Mix (Life Technologies, Paisley, UK) by QuantStudio™ 5 and 6 Pro Real-Time PCR System (Life Technologies, Paisley, UK). To determine the relative expression, three replicates were used based on a $2^{-\Delta\Delta Ct}$ method for fold change determination. Probes of TaqMan® assays provided by Applied Biosystems are listed in the supplementary table S4B.

### *2.4. Whole Transcriptome Sequencing (RNA-seq)*

The total RNA of different conditions of HCT116 cells and their quality and quantity were isolated using the previously mentioned RNA extraction section. 1 μg of RNA from each sample was used after rRNA depletion on an Illumina NovaSeq 6000 high throughput next generation sequencing (NGS) platform (Novogene, Cambridge, UK) for whole-transcriptome sequencing. Three biological replicates for the WT and KO were prepared, and two replicates for the samples treated with EZH2 activity inhibition were prepared.

### *2.5. RNA Sequencing Data Analysis*

The acquired 150 bp paired-end reads were aligned to the GRCh38 human transcriptome by using and applying HISAT2, according to Kim et al. 2019 [34]. Aligned reads are converted to BAM format, followed by sorting and indexing using the samtools [35]. The Cufflinks program package (cufflinks, cuffmerge, cuffquant, cuffdiff) [36] was utilized to conduct transcriptome assembly and differential expression analysis. Changes in expression levels were computed by comparing the FPKM (fragments per kilobase of exon per million mapped fragments) values of the wild-type and knockout samples. Variations are represented as base two logarithms (log2 fold change) of the ratio between the knockout and the wild-type samples. Heatmaps and volcano plots were generated by the CummeRbund R package [37] and GraphPad Prism 8.0.2 software (GraphPad Software, San Diego, CA, USA), respectively.

### *2.6. Protein Extraction and Western Blot Analysis*

HCT116 cells were washed twice with cold 1X PBS, and total proteins were extracted using an appropriate amount of RIPA buffer (1% NP-40, 1% SDS, 1% sodium deoxycholate, 150 mM NaCl, 25 mM Tris-HCl pH 7.6) with the addition of a protease inhibitor cocktail (10 μl/ml) (A32965, Life Technologies, Paisley, UK). Using a prechilled centrifuge, the cell debris was pelleted at 18.000g for 15 minutes. Protein concentration determination was carried out using the Pierce™ BCA Protein Assay Kit (23227, Life Technologies, Paisley, UK). Protein amounts of 25 to 30 μg were separated using a 4–20% gradient TGX gel (4561094, BioRad, Hercules, CA, USA) and followed by transfer to

 doi:10.20944/preprints202403.0787.v1



nitrocellulose and PVDF membranes (BioRad, Hercules, CA, USA). The membrane was blocked with 5% non-fat milk in tris-buffered saline containing 0.05% Tween-20 (TBS-T) for one hour at room temperature, consequently, the membrane was washed three times with TBS-T and incubated overnight at 4°C with different primary antibodies. Corresponding secondary antibodies (Supplementary Table S4A) were used and incubated for 1 hour at room temperature after three washing steps with TBS-T. Enhanced chemiluminescence (ECL) reagent (1705061, BioRad, Hercules, CA, USA) was used to develop the membranes, and the signals generated were captured using the ChemiDocTM imaging system (BioRad, Hercules, CA, USA). The ImageJ (version 1.53) and ImageLab (version 4.1) software were applied to perform densitometry of the Western blot bands [38].

*2.7. Immunocytochemistry and Fluorescence Microscopy*

Cells were seeded at a density of 35,000 cells per well onto a rounded cover slip (VWR, Leicestershire, UK). Once confluence had reached 80%, the media was drained, and three washes were carried out with 500 L of pre-warmed 1X PBS on the cells. The cells were fixed for 15 minutes at room temperature in a 4% paraformaldehyde solution. Following a second round of washing, the cells were blocked at room temperature for one hour using 500 µl of complete blocking solution (0.2% gelatin, 2% BSA, 5% FBS, and 0.1% TritonX-100 completed with 1X PBS). Subsequently, the cells were incubated at 4°C overnight with the corresponding appropriate primary antibodies, as specified in the supplementary table S4A. Following incubation, the cells were incubated with the corresponding secondary antibodies for one hour at room temperature after being rinsed three times with 1X PBS. DAPI was applied to stain nuclei (Merck KGaA, Darmstadt, Germany). A confocal microscopy system ZEISS LSM-710 camera was used to capture the images (Carl Zeiss Microscopy Gmbh, Jena, Germany). ZEN 3.2 software was utilized for image processing (Carl Zeiss Microscopy Gmbh, Jena, Germany).

*2.8. Chromatin Immunoprecipitation Sequencing (ChIP-seq)*

ChIP-seq was performed according to the manufacturer's protocol using the Pierce™ Magnetic ChIP Kit (Life Technologies, Paisley, UK). Cells were sonicated at 18 cycles, 30s ON/30s OFF (high setting) using the Bioruptor (Diagenode). The cell lysates were incubated overnight at 4 °C with H3K27me3 Monoclonal Antibody (G.299.10) ChIP-Verified (Life Technologies, Paisley, UK) and rabbit IgG (Sigma) negative control antibody provided by the kit. 1 µg of DNA of each sample was sent for the construction of a cDNA library for Illumina high throughput NGS sequencing (Novogene, Cambridge, UK).

*2.9. Chip-Seq Data Analysis*

As a first step, we performed quality control with FastQC [Andrews, S. (2010) FastQC: A Quality Control Tool for High Throughput Sequence Data (online)]. Available online at: http://www.bioinformatics.babraham.ac.uk/projects/fastqc/]. The KO sample contained a considerable amount of adapter sequences, so Trimmomatic, a read trimming tool [PMID: 24695404], was used to eliminate them. The sequenced reads (in Fastq format) were mapped to the human reference genome GRCh38 (version GRCh38.d1.v1) using BWA-MEM (version 0.7.1) [PMID: 20080505]. The aligned SAM files were converted to BAM files using SAMtools View (version 1.10) [PMID: 19505943], the BMA files were sorted with SAMtools sort and indexed with SAMtools index. Duplicates (reads located at the exact same location) were marked using Picard tools MarkDuplicates (version 1.100) [http://broadinstitute.github.io/picard/]. For visualization of chipseq data coverage files were created which show read numbers per genomic regions using deepTools bamCoverage (version 3.1.3.) [PMID: 27079975]. RPGC (Reads Per Genomic Content) normalization method was applied. In order to get information about the methylation in the promoter regions, read density plots and heatmaps were created around TSS. To achieve that we first created an intermediate matrix file

 doi:10.20944/preprints202403.0787.v1



using deepTools computeMatrix. Heatmaps combined with read density profiles were created using deepTools plot Heatmap.

*2.10. Cell Migration Assay*

The cell migration assay was carried out using μ-Dish culture-insert 2 well (Ibidi GMBH, Gräfelfing, Germany). Following the manufacturer's instructions, 7x104 cells were placed in culture-insert dishes and allowed to incubate until they attained full confluency. Subsequently, the plastic inserts were taken out and the dishes were rinsed using PBS and resupplied with 1 ml of McCoy's 5A complete medium (Life Technologies, Paisley, UK) before being placed in an incubator at a temperature of 37°C to facilitate the wound closure. The LEICA DMi1 inverted microscope (Leica Microsystems GmbH, Wetzlar, Germany) was used to capture images at 0 hr., 24 hrs., and 48 hrs.

*2.11. Transwell Invasion Assay*

A cell invasion assay was carried out for HCT116 wild-type and knockout using BioCoat® Matrigel® Invasion Chambers (Corning Inc., NY, USA). In the upper chambers, cells were seeded at a density of 2.5 x 104 filled with McCoy's 5A serum-free medium and incubated for 48 hours. As a chemoattractant, 5% FBS was added to the lower chamber. Using a cotton-tipped swab, the cells on the inserts' upper surface were removed after 20, 40, and 60 hours of incubation time, and the cells presented on the bottom surface of the insert were fixed with 100% methanol, followed by staining with crystal violet. Images were captured with a Leica DMi1 inverted microscope. Invasion efficiency was determined by invading cells counted in 10 random fields at 10X objective lens magnifications and analyzed.

*2.12. Cell Proliferation Assay*

In a 24-well plate, 1x105 cells were seeded, each containing 1 ml of McCoy's 5A complete media. Following adhesion, cells were washed twice with 1X PBS, fixed with a 10% formalin solution, and marked as day 0. From days 2 to 5, cells were fixed daily. Cells were washed three more times with PBS and then left to dry. 500 μl of 0.5 crystal violet (C0775, Merck KGaA, Darmstadt, Germany) was used to stain the cells. crystal violate resolubilized by adding 10% acetic acid (Merck KGaA, Darmstadt, Germany) to each well. At 595 nm, the absorbance was read using a SynergyMX plate reader (BioTek Instruments, Windooski, VT, USA).

*2.13. Viability Assay*

The viability of cells was determined by adding equal volumes of 0.4% trypan blue dye to the cells suspended in serum-free McCoy's 5A medium, followed by an incubation of three minutes at room temperature. A hemocytometer counter was used to count the cells using a Leica DMi1 inverted microscope. The percentage of viable cells was determined by calculating the number of viable cells divided by the number of total cells.

*2.14. Statistical Analysis*

An unpaired Student's t-test was performed to analyze the statistics of the experimental data, GraphPad Prism 8.0.2 software was used (GraphPad Software, San Diego, CA, USA).

**3. Results**

*3.1. Elevation of H3K27me3 in TKS4 KO Cells*

In our previous work [33], we demonstrated that the removal of TKS4 results in a fundamental reorganization of several different signaling pathways, which was accompanied by large-scale changes in the transcriptome of the TKS4 KO human colorectal cancer (HCT116) cells. In our pursuit to understand the molecular mechanisms behind these changes, our attention was drawn to EZH2, an important regulator of gene expression, whose effects are similar to the phenotypic changes

 doi:10.20944/preprints202403.0787.v1



observed in the KO cells, and the Cancer Genome Atlas (TCGA) database revealed that the EZH2 expression was 2.4 times higher in colon cancer compared to normal cells [39]. Therefore, we compared the activity of EZH2 in the WT HCT116 and the TKS4 KO cells using Western blot, immunocytochemistry (ICC), and Chromatin Immunoprecipitation (ChIP-Seq) against the H3K27me3 mark. Our results, represented on Figure 1A showed that the global H3K27me3 level was elevated in the TKS4 KO cells, with an approximately 1.3 fold increase compared to the WT cells. An increased H3K27me3 intensity could also be observed by ICC (Figure 1B), where the H3K27me3 labeling resulted in stronger signals in the KO cells than in the WT. While the 1.3 fold increase is not a dramatic change, it can still lead to altered gene expression and its effects can be propagated throughout the proteome if key regulators are affected. Our ChIP-seq results confirmed these alterations, as we could detect a similar elevation in the H3K27me3 mark in the promoter region of genes (Figure 1C and Supplementary Figure S1C). Importantly, these changes were not a result of an increased availability of EZH2, as the RNA expression and protein level of EZH2 appeared to be unchanged, indicating that the higher methylation level was due to its increased activity (Figure 1A and D). The observed changes in H3K27me3 levels were not accompanied by a general increase in protein methylation, as a Western blot with mono-methyl lysine antibody confirmed that the monomethylated lysine levels were unchanged in the KO cells, compared to the WT (Figure 1E).

### *3.1. The Absence of TKS4 Induces Migration and EMT-like Changes through EZH2 Hyperactivity*

The deletion of TKS4 generated numerous morphological alterations in the HCT116 cells, in keeping with the previously documented EMT-like characteristics [9,33]. To determine if there is a causal relationship between the observed morphological changes and the activation of EZH2, we applied an EZH2 activity inhibitor treatment. 1 μM DZNep treatment resulted in a significant reduction of H3K27me3 levels in both the WT and the KO cells (Figure 1A), indicating the efficiency of the treatment. Reducing the activity of EZH2 resulted in a reversal of the increased migratory speed of the KO cells, while it was much less effective in the WT cells. Compared to the WT cells, the TKS4 KO cells demonstrated a 30% increase in wound closure after 48 hours, while this difference was reduced to 10% between the KO and WT DZNep treated cells (Figure 2A and Supplementary Figure S2A). Even more importantly, the inhibitor treated KO cells showed similar behavior to the WT cells, indicating that EZH2 inhibition could counter the effects of TKS4 deletion. The fact that there was no significant difference in the behavior of the non-treated and treated WT cells suggests that the observed effects are linked to the absence of TKS4 and not an inherent consequence of EZH2 inhibition.

The increased motility of the TKS4 KO cells was accompanied by a downregulation of epithelial markers such as e-cadherin (CDH1) [40], claudin (CLDN) [41], occluding (OCLN) [42], tight junction protein (TJP1) [42,43], cytokeratin (KRT7) [44], and connexin (CNST) [45,46] and an increase in the expression level of most mesenchymal markers, such as fibronectin-1 (FN1) [47], vimentin (VIM) [48], snail (SNAI1) [49], slug (SNAI2) [50], twist (TWIST) [51], Matrix metalloproteinases (MMPs) and ZEBs (ZEB1) [52] (Figure 2B and Supplementary Figure S2B). On a whole-transcriptome level, RNA-seq data indicated that about 80% of well-known EMT markers are changed upon deletion of TKS4. These changes are mostly restored when EZH2 activity is inhibited in the KO cells (Figure 2C and supplementary tables S1A and S2). Treating the WT cells with an EZH2 inhibitor generally increases the expression of epithelial markers and decreases the mesenchymal markers, as shown in the EMT section of Supplementary Table S1.

Targeted qPCR measurements confirmed the findings of the transcriptomic analysis, (Figure 2D): epithelial markers generally showed a reduced expression in the KO cells and mesenchymal markers were dramatically increased, and EZH2 inhibitor treatment could largely reverse these alterations. In the case of the WT cells, inhibitor treatment resulted in a milder, but similar outcome, indicating that the EMT-like changes observed in the TKS4 KO cells are directly related to the activity of EZH2.

 doi:10.20944/preprints202403.0787.v1



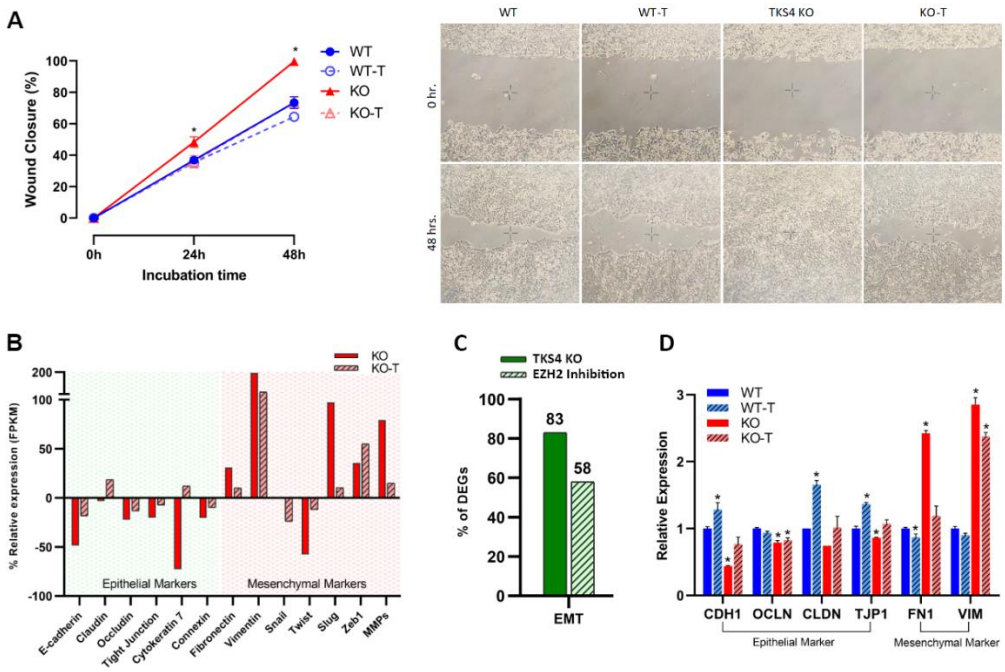


**Figure 2.** Effects of TKS4 and EZH2 inhibition on cell motility. (**a**) Left: migration speed (n = 3) of the WT (blue), WT-T (dotted line, empty circles), KO (red), and KO-T (dotted line, empty triangles) cells. Right: representative wound healing assay images showing cell migration of HCT116 cells in 0 hours after plastic inserts were removed (top row) and 48 hours after plastic inserts were removed (bottom row). (**b**) Relative expression of epithelial and mesenchymal markers based on transcriptome sequencing data. The expression of the genes in the untreated WT cells was set to 0. (**c**) Percentage of Differentially Expressed Genes (DEGs) in the KO and the KO-T cells. (**d**) Expression levels of epithelial and mesenchymal markers based on q-PCR experiments (n = 3). Results significant at p > 0.005 are marked with an asterisk.

### *3.3. Absence of TKS4 Induces Invasion through EZH2 Hyperactivity*

The absence of TKS4 not only increased the speed of migration but also enhanced the capability for invasion, with the number of invading cells doubling by 60 h in the case of TKS4 KO cells, compared to the WT. In line with the known involvement of EZH2 in the invasion of cancer cells [53], EZH2 inhibition significantly reduced the invasion capacity of both the WT and the KO cells (Figure 3A and supplementary Figure S3A).

According to the transcriptomic analysis, a noticeable elevation could be observed in the expression of most of the invasion marker genes (Figure 3B and Supplementary Figure S3B), such as urokinase-type plasminogen activator (PLAU) [54], laminin genes (LAMA3, LAMA5) [55–57], Collagen related genes (COL1A1, COL4A3, and COL6A2) [58–61], cathepsin genes (CTSA, CTSB) [62–64], serpine1 (PAI-1) [65], MMP genes (MMP7, 9, 13, 14, and 17) [66–70] [55–60], and integrin related genes (ITGA2, ITGA3, and ITGB4) [71–73]. The analysis also revealed that over 85% of recognized invasion markers undergo alterations upon TKS4 deletion, and around 75% of these changes are reversed by the inhibition of EZH2 activity. (Figure 3C and Supplementary Tables S1.A and S2.). Quantitative measurements confirmed an increase in the expression level of an invasion marker, urokinase-type plasminogen activator (PLAU) (increase above 2.5-fold) and MMP9, which decreased significantly upon EZH2 inhibitor treatment. On the other hand, they also indicated a strong downregulation of MMP14 expression in TKS4 KO cells that couldn't be changed with the inhibitor treatment (Figure 3D).

 doi:10.20944/preprints202403.0787.v1



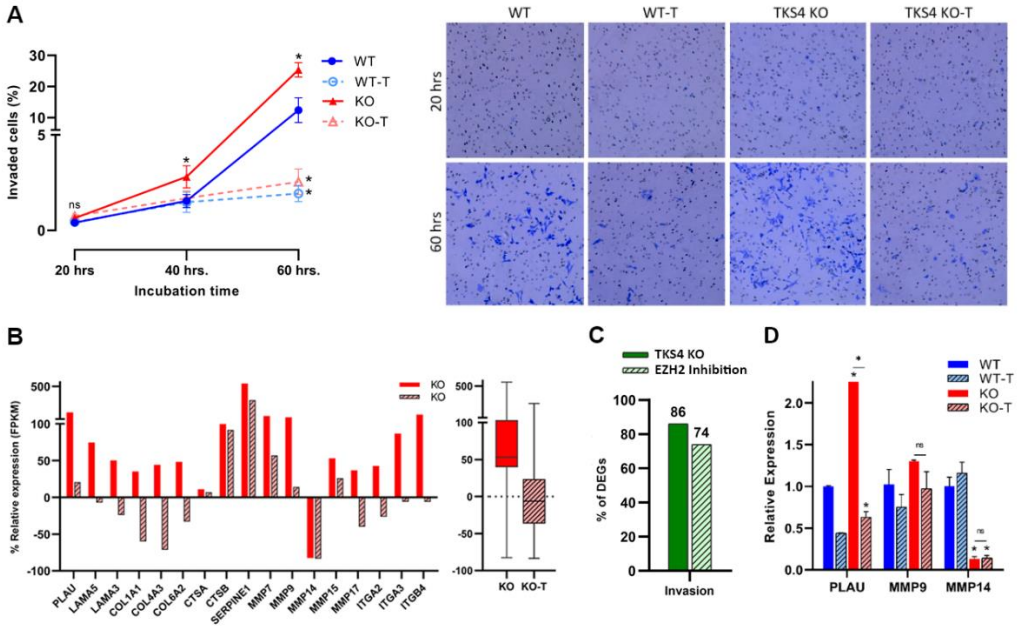


**Figure 3.** Effects of TKS4 and EZH2 inhibition on the invasion capacity. (**a**) Left: invasion speed of the WT (blue), WT-T (dotted line, empty circles), KO (red), and KO-T (dotted line, empty triangles) cells. Right: representative invasion assay images showing the number of invaded cells in 20 hours after cell seeding (0 hours after the cells on the upper surface of the inserts were removed) (top row) and 60 hours after cell seeding (bottom row). Original invasion assay images are presented in File S3. (**b**) Left: relative expression of individual invasion markers based on transcriptome sequencing. Right: relative expression (FPKM) of total invasion markers based on transcriptome sequencing. (**c**) Percentage of DEGs in the KO and the KO-T cells. (**d**) Expression levels of invasion markers based on q-PCR experiments (n = 2). Results significant at $p > 0.005$ are marked with an asterisk.

### *3.4. EZH2 Inhibition Decreases Proliferation Rate*

Surprisingly, the cells lacking TKS4 exhibited a notable decrease in cell proliferation rate while simultaneously experiencing an increase in cell motility and invasion potential. During a 5-day proliferation assay, both wild-type (WT) and knockout (KO) cells exhibited comparable rates of proliferation until the second day following adhesion. However, the proliferation of the KO cells significantly decelerated starting on the third day, resulting in a drop of about 40% by the fifth day. Contrary to other morphological changes, the EZH2 treatment could not reverse these effects, as the proliferation rate was further reduced after treatment of both wild-type and TKS4 KO cells (Figure 4A). Transcriptomic data demonstrated that the TKS4 KO cells exhibited a decrease in the expression of key proliferation promoter genes, such as Marker of proliferation Ki-67 (MKI67) [74], cyclin-dependent kinase genes (CDK1, CDK2, CDK6, CDK7, and CDK8) [75–79], Cyclin A (CCNA) [80], Cyclin C (CCNC) [81], Cyclin D1 (CCND1) [82], and minichromosome maintenance complex components (MCM2, MCM4, and MCM9), and EZH2 inhibitor treatment resulted in further downregulation (Figure 4B). At the same time, proliferation inhibitors, such as cyclin-dependent kinase inhibitors (CDKN1A, CDKN1B, CDKN1C, CDKN2A, and CDKN2B) [83,84] showed increased expression, which was even more pronounced when EZH2 activity was inhibited (Figure 4B and Supplementary Figure S4). The gene expression levels of MKI67 [85] exhibited a reduction of around 20% in TKS4 knockout cells; however, this decrease remained statistically unchanged following the EZH2 inhibitor treatment. The expression levels of CCND1 [86] and CDK6 [87] exhibited a reduction of around 25% and 40%, respectively, which were further reduced when EZH2 activity was inhibited (Figure 4D). On a global level, around 75% of the widely recognized proliferation markers face changes when TKS4 is deleted, and only roughly 20% of these are restored by EZH2 inhibition (Figure 4C, supplementary tables S1A and S2).

 doi:10.20944/preprints202403.0787.v1



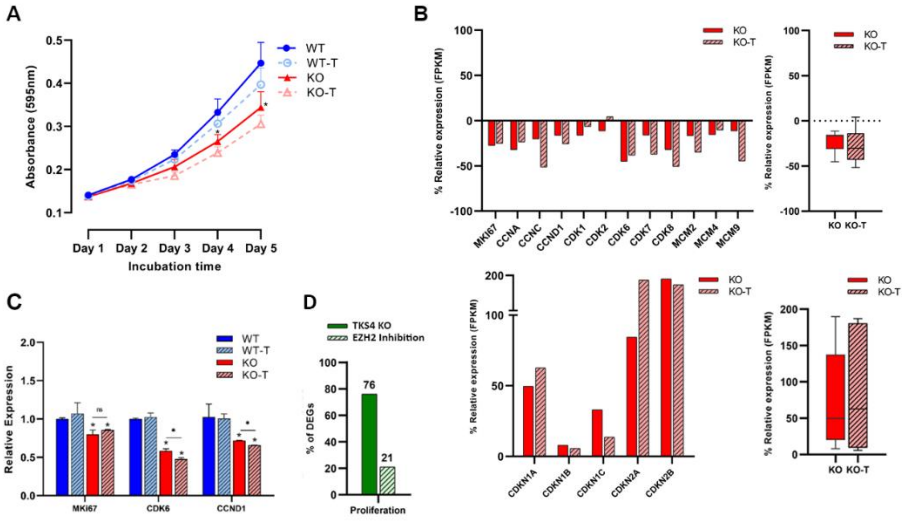


**Figure 4.** Effects of TKS4 and EZH2 inhibition on proliferation. (**a**) Proliferation rates of the WT (blue), WT-T (dotted line, empty circles), KO (red), and KO-T (dotted line, empty triangles) cells (n = 3). (**b**) Top left: relative expression of the individual proliferation promoter genes based on transcriptome sequencing. Top right: relative expression of total proliferation promoters based on transcriptome sequencing. Bottom left: relative expression of individual proliferation inhibitors based on transcriptome sequencing. Bottom right: relative expression (FPKM) of total proliferation inhibitors based on transcriptome sequencing. (**c**) Expression levels of selected proliferation markers based on q-PCR experiments (n = 2). (**d**) Percentage of DEGs in the KO and the KO-T cells. Results significant at $p > 0.005$ are marked with an asterisk.

### *3.5. Effects of TKS4 and EZH2 Inhibition on Global Gene Expression*

Approximately 6000 protein-coding genes exhibited a minimum of 25% gene expression alteration following the removal of TKS4, of which 3789 genes were upregulated and 2463 were downregulated, implying a substantial reorganization of the regulation of gene expression following TKS4 deletion. On top of these changes, there are several genes that are only expressed in a particular cell type: 196 and 187 genes were only expressed in WT and KO cells, respectively, while 349 genes were specific to WT-T, and 212 genes were specific KO-T cells (Figure 5A, Venn diagram). We also found 142 mRNAs exclusive to the treated cells, suggesting that these genes are strictly regulated by EZH2. As expected, the EZH2 inhibitor-treated samples were characterized by a wider gene expression pattern, compared to the untreated cells (Figure 5A, heatmap). 841 protein-coding genes were significantly downregulated with a log2 fold decrease greater than 1.3 in the TKS4 KO cells, and 1250 were upregulated with a similar efficiency in response to EZH2 inhibition, compared to the WT cells (for details, see Supplementary Table S2).

Several important regulatory genes were significantly downregulated in the KO cells (MAGI2, PNLDC1, CLMP, and GRHL3) that responded to the EZH2 inhibitor treatment (Figure 5B); many of which are involved in epithelial differentiation [88–91]. We could detect upregulated genes as well (PLAU, SERPINA1, and AKT3), mainly connected to cancer development and progression and mesenchymal phenotypes, that were also responsive to EZH2 inhibition (Figure 5B). The genes belonging to the first group are most probably under the direct control of PRC2 activity, while PRC2 likely regulates the expression of a transcriptional inhibitor in the case of the second.

The presence of several genes unresponsive to EZH2 inhibition indicates that other regulatory mechanisms are connected to TKS4, besides PRC2. Some downregulated genes (EHF and MMP14), mainly involved in proliferation and cancer development, were not restored upon EZH2 inhibitor treatment, and some that were upregulated in KO samples retained or even increased their high expression after treatment (EFCAB6 and CDKN2A) (Figure 5B).

 doi:10.20944/preprints202403.0787.v1



This latter observation offers an explanation why the proliferation rate was not increased in the EZH2 inhibitor-treated cells. To confirm these findings, some selected genes were also investigated by quantitative PCR (Supplementary Figure S5.). The expression of the glucose transporter SLC2A1 (like other proteins belonging to the same family - see Supplementary Table S2.) was significantly reduced in the TKS4 KO cells, suggesting that TKS4 plays a role in the signaling pathways that contribute to cancer progression. HOXB7, which controls proliferation and differentiation, was also downregulated. The fact that neither of these changes could be reversed by the addition of an EZH2 inhibitor highlights the importance of other, PRC2 independent regulatory pathways connected to TKS4.

As opposed to SLC2A1 and HOXB7, the expression of AKT3 (RAC-gamma serine/threonine-protein kinase) and PLAU increased strongly in the TKS4 KO cells and were reduced when the KO cells were treated with the EZH2 inhibitor (Supplementary Figure S5 and Figure 3D). This could suggest that EZH2 controls the expression of a negative regulator, thus the changes in its activity manifest in reverse in the expression of AKT3 and PLAU.

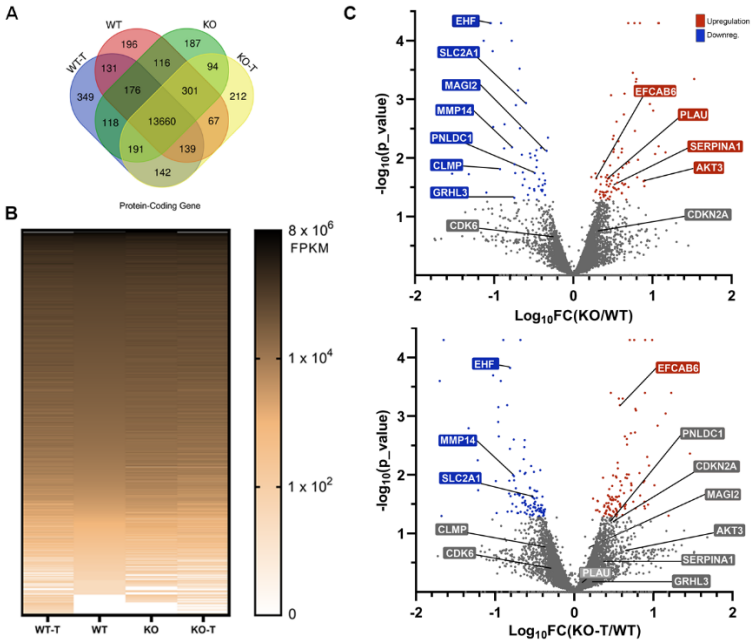


**Figure 5.** Transcriptome-level changes in mRNAs. (**a**) The Venn diagram of the identified mRNAs in the different cell lines and treatments. (**b**) Heatmap visualization of the DEGs in the different cell lines and treatments. (**c**) Volcano plot of the mRNA expression changes in the KO (top) and the KO-T cells (bottom), with colored points representing significantly up- (red) or down- (blue) regulated genes ($\log_{10}$ p-value ≥ 1.3).

### *3.6. Alterations in Signaling Pathways*

Analysis of the KEGG signaling network revealed that the loss of TKS4 mostly impacts the PI3K/AKT signaling pathway, which aligns with the predicted function and molecular interactions of TKS4 [2]. A major disruption of this cascade can be determined by the greater number of downregulated genes compared to upregulated genes (Figure 6A). However, in response to EZH2 inhibitor treatment, the alterations shifted to the direction of upregulation of genes related to this pathway, indicating the involvement of TKS4 and EZH2 in proper PI3K/AKT signaling. This is also true for the calcium, Ras, Rap1, cAMP, MAPK, AMPK, and Wnt signaling pathways. The genes associated with the JAK/STAT pathway exhibit a relatively balanced up- and downregulation of its participant proteins, however, it is also switched to upregulation following EHZ2 inhibitor treatment. Phospholipase D, HIF1, and Fox0 pathways also exhibit similar behavior. Apelin, Hippo, and cGMP pathways are less sensitive to the absence of TKS4, and they did not show alterations upon EZH2 inhibitor treatment either. The genes related to mTOR, NFkB, ErbB, and TNF signaling are mostly

 doi:10.20944/preprints202403.0787.v1



upregulated, and the perturbation is reduced upon treatment, suggesting that EZH2 may play a negative regulator role of these pathways in HCT116 cells. Notch, VEGF, TGF-beta, and sphingolipid pathways are little affected by the deletion of TKS4, with a small number of differentially expressed genes, but most of these are upregulated (Figure 6A). Interestingly, while hedgehog and sphingolipid signaling seem to be rather insensitive to the absence of TKS4, they show relatively strong reactions to the inhibition of EZH2 activity (Figure 6A). It is important to highlight that the ultimate outcome of abnormal gene expression cannot be determined solely based on the number of suppressed or elevated genes in a signaling pathway, as the changes in the expression of repressor or activator genes can have contrasting impacts on the overall functioning of the pathway.

As a consequence of the significant alterations in gene expression exhibited in KO cells, various cellular processes are disrupted. Unsurprisingly, signal transduction exhibited the highest number of perturbed genes with a higher proportion of downregulated examples. EZH2 inhibition appeared to reverse these changes, shifting the balance to the upregulation side. The same could be observed in processes like developmental biology, metabolism, gene expression (transcription), post-translational modification and Receptor Tyrosine Kinase (RTK) signaling pathways. Remarkably, the TKS4 KO cells exhibited a decrease in the expression of DNA repair and chromatin structure genes, indicating a compromised ability to respond to cellular stress. Cellular senescence, while not among the most affected processes, exhibits more upregulation than downregulation, and no notable alteration is found following the treatment (Figure 6B). Furthermore, our findings indicate that around 65% of widely recognized indicators of senescence exhibit at least 20% alterations in their expression (Supplementary Figure S6), and approximately 15% of them show reactions to EZH2 inhibition (Figure 6C). Splicing and splicing factor markers (Figure 6C, right, and Supplementary Table S1) represent similar behavior upon TKS4 deletion and subsequent EZH2 inhibition. The processes that involve the most genes with altered expression in the TKS4 KO cells are, unsurprisingly, EMT and invasion, and both show strong reactions to EZH2 inhibition (Figure 6C, left).

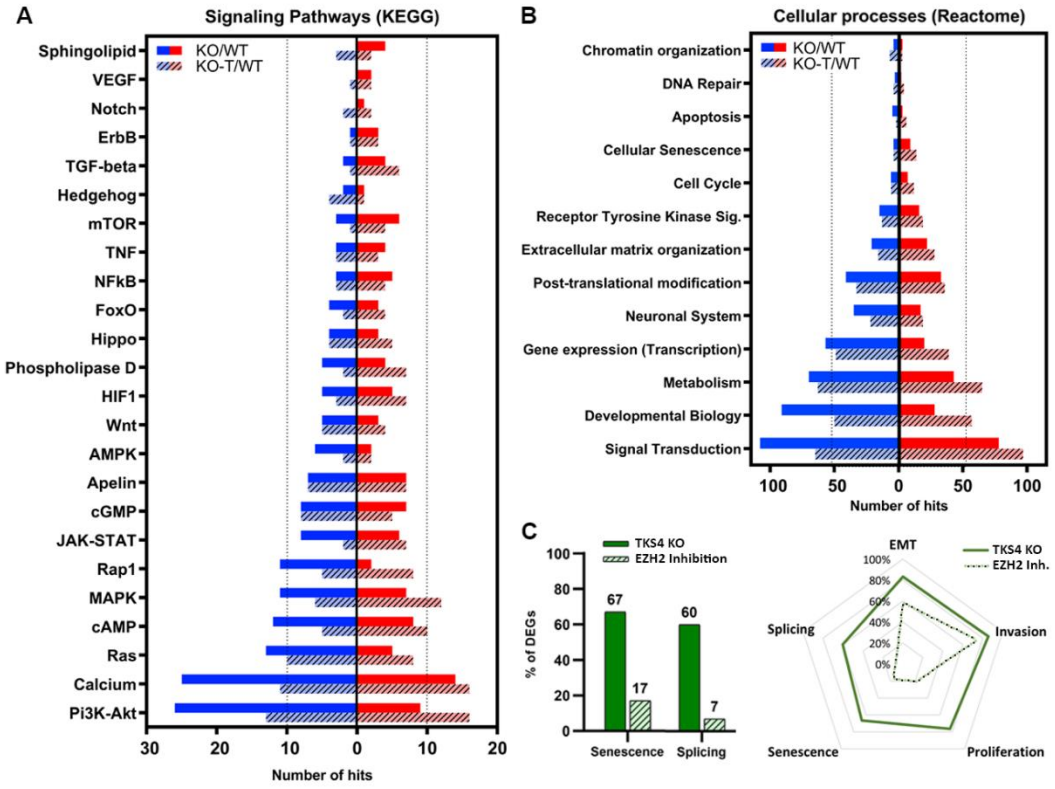


**Figure 6.** KEGG pathway and Reactome analysis of the transcriptomic changes.(a) The effects of TKS4 deletion and EZH2 inhibition on the signaling pathways. (b) Effect of TKS4 deletion and EZH2

 doi:10.20944/preprints202403.0787.v1



inhibition on cellular processes. Upregulation is indicated by red, whereas downregulation is indicated by blue. EZH2 inhibitor treatment is indicated by dashed columns. (c) Percentage of DEGs in the KO and the KO-T treated cells. Area of alteration of genes involved in different processes when TKS4 is absent and EZH2 is inhibited. The analysis only included genes that exhibited a minimum two-fold change in expression, either through downregulation or overexpression.

### *3.7. Changes in Long Non-Coding RNAs*

In recent decades it has been demonstrated that non-coding RNAs (ncRNAs) that do not possess protein coding capacity, play a significant role in regulating different biological processes, a relevance comparable to protein coding genes. A large group of ncRNAs are long non-coding RNAs (lncRNAs) that have a length above 200 nucleotides [92], containing more than 100.000 representatives in the human genome [93]. Numerous observations underline their involvement in cancer development and progression [94], and several of them are regarded as novel biomarkers for cancer diagnosis and prognosis [95].

To gain a deeper understanding of the disruptions caused by the TKS4 knockout, we examined the expression of lncRNAs both in WT and TKS4 KO cells. We identified 1870 lncRNAs that were present in our transcriptomic datasets in any of the investigated cell types (Supplementary Table S3). A total of 83 lncRNAs were exclusively identified in WT cells, whereas 165 lncRNAs were only found in KO cells. Additionally, 124 lncRNAs were detected only in WT-T cells, and 89 lncRNAs were only present in KO-T cells (Figure 7A). A heat-map based on the transcriptomic data (Figure 7A, lower panel) indicates similar large-scale reorganization in the expression of lncRNAs as was seen in the case of mRNAs (Figure 5A). Interestingly, while TKS4 KO resulted in the overexpression of several mRNAs, this effect was not as pronounced in lncRNAs. The role of EZH2 in the regulation of lncRNA expression is indicated by the several lncRNAs appearing in the EZH2 inhibitor-treated samples (Figure 7A, heatmap).

However, we discovered that the loss of TKS4 led to the overexpression or downregulation of many lncRNAs that have already been linked to the development of cancer (Supplementary Table S3).

MALAT1 is known for its high expression levels in different ccancers,and it was among the most abundant lncRNAs in the WT HCT116 cells (Figure 7.B, Supplementary Table S3, and Supplementary Figure S7A), and its expression is further increased in TKS4 KO cells. Its RNA level is decreased upon EZH2 inhibition, just like NEAT1, NORAD and BCAN-AS1 (Figure 7.B). HOTAIR, a well-known molecular partner of EZH2 that is involved in the regulation of EMT [24,96], was overexpressed in the TKS4 KO cells, and its expression was further increased upon EZH2 inhibition.

The lncRNAs whose expression was downregulated in TKS4 KO cells and were induced upon EZH2 inhibition include Mir4435-2HG, LINC01234, and TERC (Figure 7.B). The expression of LINC01123 and LINC01405 was reduced in the TKS4 KO cells and remained unchanged after EZH2 inhibitor treatment, indicating an EZH2-independent regulation. The loss of TKS4 led to a decrease in the expression of lncRNAs, such as LINC02575, HAGLR, LINC00222, and HOTTIP but they did not react the same way to the EZH2 inhibition. LINC02575 and HAGLR did not show significant changes, the expression of LINC00222 was further decreased and HOTTIP expression was restored upon treatment. The expression of selected lncRNAs was confirmed with a quantitative qPCR which resulted in identical results as those provided by the RNA-seq data (Figure 7C, Supplementary Table S3, and Supplementary Figure S7B).

 doi:10.20944/preprints202403.0787.v1



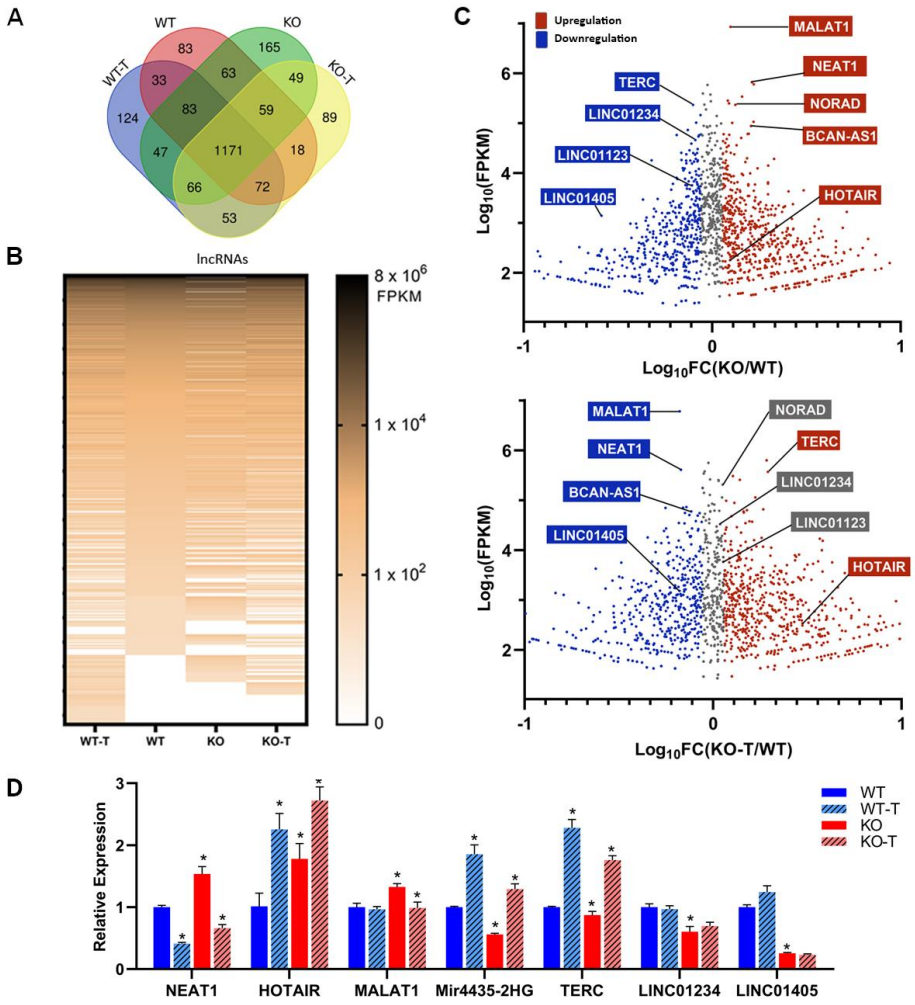


**Figure 7.** Transcriptomic changes in lncRNAs. (**a**) The Venn diagram and (**b**) Heatmap illustrate the changes in non-coding genes generated by TKS4 KO and EZH2 inhibitor treated cells. (**c**) Several lncRNAs show altered expression levels after TKS4 deletion (top), while EZH2 inhibition restores the expressions in many examples (bottom). (**d**) Quantitative analysis showing fold-change of the different lncRNAs. Results significant at $p > 0.005$ are marked with an asterisk.

## 4. Discussion

The TKS4 KO cells displayed diverse expression levels of several conventional EMT markers. Proteins specific to epithelial cell types such as CDH1, cytokeratin, occludin, and TJP1/2 are reduced in expression, but most of them are recovered after treatment. Meanwhile, mesenchymal markers such as FN1, VIM, Zeb1, and SNAI2 show increased expression, according to the sequencing data. However, Twist1 and N-cadherin are downregulated, and no alteration was found in the EMT main marker, snai1. These alterations suggest a partial EMT (pEMT) and align with previous findings involving the TKS4 KO cell line [9]. We proposed that the hyperactivity of EZH2 is responsible for the induced p-EMT because the gene expression of most genes was restored after treatment of EZH2 activity inhibition. Both EZH2 and EMT are intricately linked, as stated in the literature. EZH2 has been shown to enhance EMT by interacting with SNAIL1 and reducing the expression of E-cadherin [97,98]. EZH2 can promote gene silencing of Disabled Homolog2-Interacting Protein (DAB2IP) to control EMT and metastasis in colorectal cancer cells [99]. MMPs play a significant role in promoting EMT and invasion and are mostly upregulated in TKS4 KO cells, they are predominantly restored upon the EZH2 inhibitor treatment, despite MMP13 and MMP14 showing decreased expression.

In addition to the pEMT, the EZH2 overactivation led to invasion in TKS4 KO cells. This is expected since the first step of undergoing invasion is usually EMT. Besides the invasion assay, we

 doi:10.20944/preprints202403.0787.v1



observed that most of the invasion markers were upregulated in the TKS4 KO sample and restored in the KO-T sample, indicating the role of EZH2 in cell invasion. EZH2's role in the invasion is mostly correlated with the literature, in which EZH2 is shown to enhance tumor cell invasion. EZH2 suppresses TIMP2 expression through H3K27me3, leading to the MMP stimulation that leads to migration and invasion in ovarian cancer cells [100] and through MMP2 and MMP9 in triple-negative breast cancer (TNBC) cells [101]. EZH2 plays a role in controlling cell migration and invasion by regulating the expression of TGF-β1 [102]. EZH2 mediates the activation of EMT and invasion, leading to increased metastasis in several cancers, including CRC, melanoma, and breast cancer.

In addition to migration, pEMT, and invasion, there are numerous established markers for invadopodia and podosome formation like Lasp1 [103], paxillin (PXN), dynamin (DNM1, DNM2, and DNM3), fascin (FSCN1, FSCN2, and FSCN3), vinculin (VCL), and paladin (PALD1) [104] are upregulated, and these upregulations are mostly due to the disruption caused by EZH2 hyperactivity induced by TKS4 deletion because most of them are strongly reversed upon EZH2 inhibition treatment. While other markers such as MMP14, Zyxin (ZYX), [105], Arp2/3, and N-WASP (WASL) [106] are downregulated in the TKS4 KO cells, and cannot be restored with EZH2 inhibition, corresponding to the protein that is crucial for invadopodia [107] and podosome formation [7]. We performed an immunostaining study to show the localization of MMP14 protein upon the TKS4 deletion, we found that MMP14 is more precisely located around the nucleus of the TKS4 KO cells, with a decreased protein level compared to MMP14 observed in the spindles (invadopodia and podosome) of WT cells (Supplementary Figure S8). In combination, these findings demonstrate that the removal of TKS4 leads to a widespread decrease in the expression of genes associated with the formation of invadopodia and podosome.

Unexpectedly, the TKS4 KO cells experience a notable decrease in their proliferation rate, along with an increase in their migration and invasion. Usually, the proliferation is parallel with migration, EMT, and invasion [108]. However, both the morphological study and the gene expression alterations provided evidence of the decrease in proliferation. We found a decrease in the expression of cyclin-dependent kinases (CDKs) and an increase in the expression of cyclin inhibitor proteins (CDKNs), which are not reversed with EZH2 activity inhibition. The effect of a decrease became stronger in most proliferation markers. The TKS4 KO cells exhibit downregulation of multiple genes in the MAPK cascade, including different RAS isoforms, RAF, MEK1/2, and ERK1/2 (mainly responsible for cell proliferation), which are not affected by EZH2 inhibition, or the effect on some of them becomes more prominent after treatment (Figure 8). This indicated the decreased proliferation was due to the disruption caused by TKS4 deletion and not by EZH2 hyperactivity.

### *4.1. Signaling Pathways Reactive to EZH2 Inhibition in TKS4 KO Cells*

Removal of TKS4 leads to a major dysregulation of several signaling pathways through global alterations in gene expression, indicating the existence of intracellular factors that are involved in the spreading and amplifying the effect of its absence. Based on our results detailed above, EZH2 and through its activity, PRC2 appears to be one of these factors. A closer analysis of the signaling pathways reveals the possible molecular mechanisms of EZH2 involvement in the translation of TKS4 loss to gene expression changes. We have provided a schematic representation of the signaling pathways that are affected by the lack of TKS4, and we found that EZH2 inhibition reversed the expression of many genes, indicating the involvement of EZH2 in different signaling pathways (Figure 8).

#### 4.1.1. EZH2/PI3K/Akt Signaling Pathway

This pathway is widely recognized to be disrupted in cancer [109], and its dysregulation in the TKS4 KO cells largely accounts for the observed increase in their migration capacity. We detected an increased expression of multiple genes associated with the PI3K/Akt pathway, such as PLAU, PAI1 (Figure 3), and AKT3 (Supplementary Figure S5), which significantly decreased when EZH2 activity was inhibited, indicating that EZH2 suppresses their negative regulator(s). PAI1 is known to induce cancer cell migration and invasion [110] while decreasing cell proliferation [111], which was observed

 doi:10.20944/preprints202403.0787.v1



in the cells lacking TKS4 (Figure 8.). The AKT3 overexpression demonstrates increased activity of this pathway, and elevated AKT3 expression is correlated with the process of EMT in colorectal cancer cells [112]. AKT3 decreased expression after treatment, indicating that controlling EZH2 activity might moderate colorectal cancer progression.

EZH2 has been implicated in PI3K/AKT signaling by several earlier studies. For one, EZH2 itself can be phosphorylated by AKT [113], which leads to an elevation of genes maintaining apoptosis [114]. EZH2, in turn, can promote the pathway through suppressing PIK3IP1 [115] and PTEN [116]. Despite being known as a transcriptional repressor, EZH2 can also facilitate gene expression, as exemplified by IGF1R. In this case, EZH2 directly binds and recruits MYC to the IGF1R promoter thus upregulating its expression, which leads to PI3K pathway activation, promoting tumor progression [117]. The AKT signaling pathway also has another, indirect effect on EZH2 expression, since it can trigger the activation of C-Jun, which leads to the binding of AP-1 to the EZH2 promoter, resulting in the elevated deposition of H3K27me3 [118]. However, this seems not to be the case in TKS4 KO cells, as we could not detect an increased expression of EZH2. The observed hyperactivity of EZH2 may be a consequence of Cell Cycle Related Kinase (CCRK or CDK20), as was observed in human hepatocarcinogenesis. CCRK induces EZH2 up-regulation and phosphorylation in an epigenetic circuitry consisting of glycogen synthase kinase 3β (GSK-3β), β-catenin, T-cell factor (TCF), E2F1, AKT, and AR, which results in enhanced CCRK transcription. This positive feedback loop was observed to contribute to hepatic tumorigenesis [119]. We observed a slight elevation in the expression of CCRK in the TKS4 KO cells (Supplementary Table S2.), but it was insensitive to EZH2 inhibition, making it unlikely that this circuit is a major contributor to the observed effects in our system.

#### 4.1.2. EZH2/JAK/STAT Signaling Pathway

The Janus kinase/signal transducers and activators of transcription (JAK/STAT) is another pathway that it promotes cell migration, cell proliferation, and differentiation [120]. In this study, we found dysregulation in many genes of TKS4 KO cells associated with this pathway, in which many of them get reversed or restored upon EZH2 activity inhibition (Figures 6 and 8). EZH2 could be linked to this pathway. EZH2 has the ability to interact with STAT3, resulting in improved STAT3 activity and impairment in this axis using specific inhibitors, resulting in decreased tumor initiation [121]. Activation of JAK/STAT3 leads to an increase in the phosphorylation of STAT3 and the phosphorylation of the 21st serine of EZH2 mediated by phosphorylated Akt, Phosphorylation of EZH2 by Akt may be a significant mechanism responsible for As3+-induced carcinogenesis in humans [122].

#### 4.1.3. EZH2/NFκB Signaling Pathway

Nuclear factor kappa B (NFκB) regulates various cellular functions, and this family of transcription factors is crucial in responding to cellular stress and regulating the expression of key genes involved in immunity, inflammation, cell death, and proliferation. [123,124]. Based on a transcriptomic study, we observed dysregulation in most of the genes connected to this pathway, many of which were reversed when EZH2 activity was inhibited, suggesting a likely association with EZH2. In a study, it was shown that EZH2-induced epigenetic suppression of DAB2IP leads to the activation of Ras and NFκB, initiating metastasis. DAB2IP is identified as a novel tumor suppressor in prostate cancer development, functioning by inhibiting the ERK and AKT pathways. EZH2 has been demonstrated to epigenetically suppress DAB2IP and stimulate AKT and NFκB [125]. It might be crucial to state that there is a 28% reduction of DAB2IP in TKS4 KO cells.

#### 4.1.4. EZH2/VEGF Signaling Pathway

Vascular endothelial growth factor (VEGF) is another signaling pathway that is one of the primary drivers of tumor angiogenesis, in which malignant cells frequently exhibit overexpression of VEGF [126]. Preclinical research suggests that the VEGF and EGFR pathways have shared parallel

 doi:10.20944/preprints202403.0787.v1



downstream signaling mechanisms. Widespread activation was noticed in the genes of the VEGF pathway in TKS4 KO cells, with many of them being reversed. We observed elevated and reversed expression of PLCγ1 (phospholipase C γ1) in TKS4 KO (Figure 8) and treated cells, respectively, that act as a signal transducer and as a direct effector of VEGFR. Some studies have linked the VEGF pathway to EZH2. A study demonstrated that overactivation of EZH2 enhances VEGF expression, and inhibiting EZH2 suppresses VEGF expression and results in inhibiting cell proliferation [127] and cell migration [128]. In another study, the VEGF pathway regulates EZH2 expression through E2F3, HIF1$\alpha$, and microRNA. Depleting EZH2 reduces the malignancy of lung adenocarcinoma [129]. EZH2 controls EMT and invasion by modulating the STAT3/VEGFR pathway, in which silencing of EZH2 results in decreased EMT and invasion of xenograft head and neck squamous cell carcinoma (HNSCC) tumors [130].

#### 4.1.5. EZH2/mTOR Signaling Pathway

Mammalian target of rapamycin (mTOR) functions as a serine/threonine protein kinase through involvement in many signaling pathways, regulates cell growth, metabolism, protein synthesis, and autophagy [131]. In TKS4 KO cells, we demonstrate more gene upregulation of this pathway and a regained WT effect in TKS4-treated KO cells (Figure 6A and 8). There are possibilities of EZH2 connection to mTOR, in which, a study indicated that the transcription factor E2F7 elevates H3K27me3 mark levels via binding to the EZH2 promoter and suppresses PTEN expression, which triggers the activation of the Akt/mTOR signaling pathway [132]. Another study shows elevated EZH2 levels are caused by the activation of mTORC1 and enhanced glycolysis in SLE CD4+ T cells [133]. EZH2 expression influences the phosphorylation of AKT/mTOR via regulating H3K27me3 and suppressing PTEN, indicating a new epigenetic mechanism in memory reconsolidation [134].

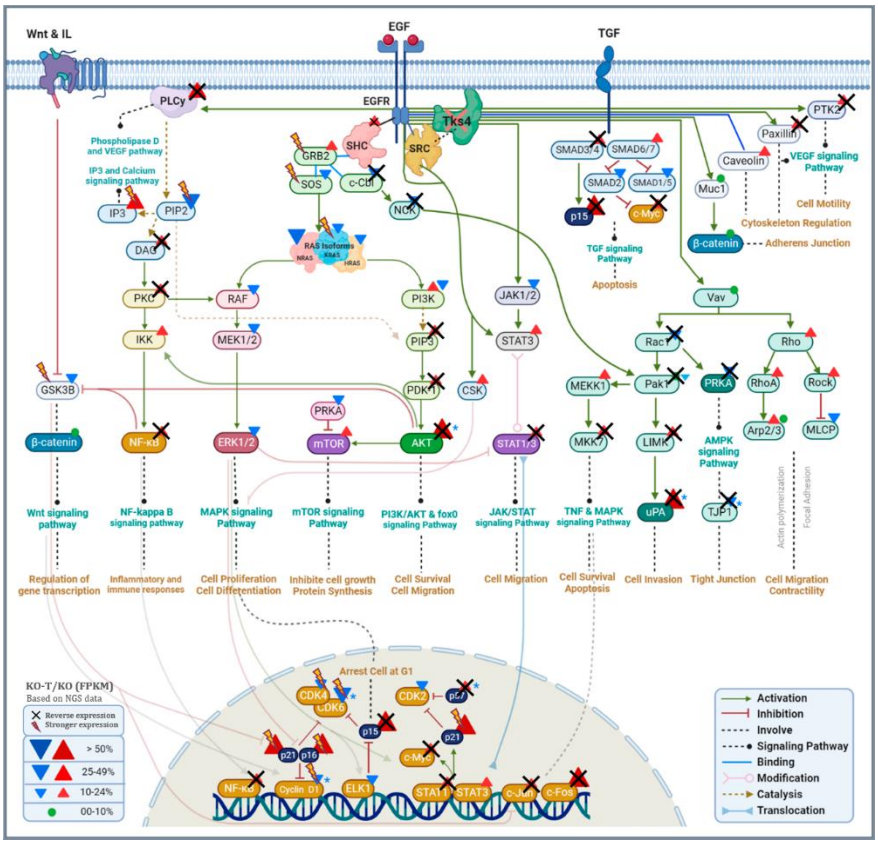


**Figure 8.** Schematic representation of the signaling pathways affected by the deletion of Tks4 and EZH2 inhibition. TKS4 deletion triggers alterations across several signaling pathways. EZH2 inhibition reversed the expression of many genes, indicating the involvement of EZH2 in these signaling pathways. Gene expression changes are illustrated by triangles, with red indicating

 doi:10.20944/preprints202403.0787.v1



upregulation and blue indicating downregulation. If both are present, they indicate alterations in distinct subunits. The cross indicates decreased expression with EZH2 inhibition, while lightning shows increased expression with EZH2 inhibition. Core genes within a certain pathway are shaded with darker colors. The diagram compares KO samples with WT samples, whereas the treatment with EZH2 inhibitor (cross and lightning) is based on comparing KO-T samples with KO samples. Gene expression changes validated by RT-qPCR are indicated by blue asterisks.

### *4.2. LncRNAs Connecting TKS4 and EZH2*

An important aspect of our study is the effect of TKS4 deletion on the expression of different lncRNAs and their connection to EZH2. Gaps in the functional annotation of lncRNAs complicate the in-depth analysis of our results in terms of possible molecular mechanisms, but a considerable number of the identified lncRNAs have already been shown to interact with EZH2 and participate in the regulation of the affected signaling pathways.

MALAT1 is known to bind to EZH2 and direct it to specific chromatin regions, leading to tumor suppressor gene repression such as e-cadherin, p21, and p27 [135–137]. It is found to enhance EMT by activating the EZH2-Notch1 signaling pathway [138], while its upregulation enhances the activity of PI3K/Akt signaling pathway [139]. The overexpression of MALAT1 in the TKS4 KO cells could be reversed by EZH2 inhibition, suggesting that EZH2 may be a negative regulator of this RNA. Importantly, the MALAT1 expression was not sensitive to EZH2 inhibition in the WT cells, indicating that EZH2 involvement in the regulation of MALAT1 expression may be related to the pathways perturbed by TKS4 deletion. Since apparently MALAT1 binding to EZH2 can inhibit tumor suppressor gene expression, overactivation of EZH2 in the KO cells may lead to a positive feedback loop, accelerating the malignant processes.

HOTAIR is another well-known lncRNA partner of EZH2, as it was suggested to regulate cell cycle progression through EZH2 [140] and it induces cell invasion and metastasis through the PRC2 complex [96,141]. HOTAIR is also involved in the upregulation of Rapamycin and PI3K/Akt signaling pathway [142]. While similarly to MALAT1, HOTAIR was also upregulated in the TKS4 KO cells, its expression was further increased upon EZH2 inhibition both in WT and KO cells. This observation suggests a complex, indirect involvement of EZH2 in the regulation of HOTAIR transcription.

NEAT1 promotes migration, invasion, metastasis, and EMT via interacting with EZH2 as a scaffold RNA [143–145], but it can also interact directly with EZH2 and recruit PRC2 to p21, Myog, Myh4, Tnni2, LATS2, and Smad7 gene promoters [146–148]. NEAT1 has been found to mainly modulate the Wnt/β-catenin signaling pathway [145] and is sensitive to EZH2 inhibition in the WT and KO cells alike, supporting a hypothesis that EZH2 regulates an inhibitor of NEAT1 expression.

Other lncRNAs with significant changes in their expression have not yet been shown to bind EZH2 itself but are known to be involved in the regulation of the signaling pathways affected by TKS4 deletion. NORAD can bind to different microRNAs and induce malignancy via PI3k/AKT/mTOR [149] and promote invasion and EMT through ERK [150] or the WNT/B-catenin signaling pathway [151]. BCAN-AS1 is suggested to interact with c-Myc through SMAD nuclear-interacting protein 1, which results in blocking c-Myc ubiquitination and degradation. Consequently, high BCAN-AS1 levels are associated with a poor prognosis [152].

Inhibition of Mir4435-2HG by microRNAs leads to invasion, migration, and EMT [153]. It triggers cancer progression through cell cycle regulators and mTOR signaling pathway [154]. A decrease in MIR4435-2HG could inhibit cell proliferation via the miR-206/YAP1 axis [155] or via modulating the Nrf2/HO-1 cascade [156] in HCT116 cell lines. In a separate study on colon cancer, the MIR4435-2HG downregulation led to the downregulation of GLUT-1 which resulted in decreased cell proliferation [157]. This is in accord with our observations as MIR4435-2HG expression is decreased in the TKS4 KO cells, where we also detected diminished proliferation rates. However, while EZH2 inhibition restored and even increased its transcription, this in itself was not enough to restore cell proliferation, indicating the importance of other regulatory mechanisms.

LINC01234 induces proliferation in colon cancer [158] and promotes malignancy through the microRNA/mTOR signaling pathway [159]. It appears to be regulated independently of EZH2, as it

 doi:10.20944/preprints202403.0787.v1



showed no significant reaction to EZH2 inhibition, and its levels were only slightly reduced in the KO cells.

LINC01123 interacts with the splicing factor SRSF7 and induces proliferation, migration, and invasion [160] in colon cancer cells. It promotes malignant behavior through the microRNA/LASP1 [161], microRNA/KIF4 [162], microRNA/PYCR1 [163], and microRNA/VEGF [164] signaling pathways.

LncRNA TERC enhances proliferation, migration, and invasion, through controlling the expression of SOX12 [165]. In our system, TERC expression appears to be inversely influenced by EZH2 activity, as it was significantly downregulated in the KO cells and EZH2 inhibition resulted in a marked upregulation of this transcript, in the WT and the KO cells alike.

LINC01405 is predicted to have a role in the regulation of Wnt, PI3K, and the TGF-beta signaling pathway [166]. Its expression was strongly downregulated in the TKS4 KO cells, and this effect could be mitigated, but not reversed by EZH2 inhibition, indicating a connection between its transcriptional regulation and EZH2.

LINC02575, HAGLR, LINC00222, and HOTTIP are involved in the KRAS [167], MAPK/AKT [168], Wnt [169], and c-Myc pathways [170], respectively.

## 5. Conclusions

The above detailed results unequivocally indicate that TKS4 deletion results in the overactivation of EZH2, which is realized in large-scale transcriptomic changes. Our analysis extended over the protein-coding transcripts, and we could identify several non-coding RNAs that are affected as well. As most of the observed phenotypic changes in cell migration, EMT, invasion and cell proliferation could be reversed or mitigated by the inhibition of EZH2 activity, we can conclude that EZH2 is directly or indirectly involved in the signaling pathways connected to TKS4. EZH2 involvement could occur as a result of redistribution of intracellular signaling molecules, like CCAR1, which is a supposed interactor of TKS4 [10], or through the dysregulated expression of EZH2-interacting molecules, like lncRNAs. As TKS4 functions as a scaffold and plays a role in the phosphorylation cascade, it might also be necessary to study the downstream phosphorylation cascade to comprehend the exact nature of this connection. However, additional research is necessary to elucidate the precise connection between TKS4 and EZH2.

**Supplementary Materials:** The following supporting information can be downloaded at the website of this paper posted on Preprints.org. Figure S1: (a) Western blotting picture of TKS4, Ezh2, H3K27me3 and Mono-Methyl Lysine (b) ICC picture showed absence of Tks4 in Tks4 KO (c) ChIP-seq data analysis (d) Western blotting picture of H3K27me3 testing two different concentrations of DZNep and viability of cells compared to different concentration of DZNep; Figure S2: (a) Migration Assay picture (b) EMT markers based on RNA-seq data; Figure S3: (a) Invasion Assay picture (b) Invasion Markers based on RNA-seq data; Figure S4: Proliferation Markers based on RNA-seq data; Figure S5: Quantitative analysis of mRNA genes confirming RNA-seq data; Figure S6: Senescence promoting and inhibiting markers based on RNA-seq data; Figure S7: Gene expression level of different lncRNA compared to GAPDH control and different LncRNAs relative expression based on transcriptomic analysis in different condition of cells compared to WT; Figure S8: ICC picture showing the localization changes of MMP14 in TKS4 KO cells compared to WT cells; Table S1: List of genes related to specific cellular processes based on log2FC, KEGG, and Reactome. Table S2: List of the differentially expressed mRNAs; Table S3: List of deferentially expressed LncRNAs; Table S4: List of antibodies and probes used in current study.

**Author Contributions:** Conceptualization, A.T.; methodology, A.T.; software, M.J and E.S.; formal analysis, M.J. and E.S.; investigation, M.J.; resources, A.T.; data curation, A.T., M.J and E.S.; writing—original draft preparation, M.J and A.T.; writing—review and editing, A.T., M.J., and E.S. ; visualization, M.J. and E.S.; supervision, A.T.; project administration, A.T.; funding acquisition, A.T. and L.B. All authors have read and agreed to the published version of the manuscript.

**Funding:** The work presented here was funded by grants K125340 and K142851 (to A.T.) from the National Research, Development, and Innovation Fund of Hungary. The APC was funded by National Research, Development and Innovation Fund of Hungary, grant number K125340 (A.T.).

**Institutional Review Board Statement:** Not applicable.

**Informed Consent Statement:** Not applicable.

**Data Availability Statement:** The datasets generated and analyzed during the current study are available from the corresponding author on request.

**Acknowledgments:** The authors would like to thank Loretta László for her help with the Confocal Microscope.

**Conflicts of Interest:** The authors declare no conflict of interest.

## References

1. Buday, L.; Tompa, P. Functional Classification of Scaffold Proteins and Related Molecules. FEBS J. 2010, 277, 4348–4355.
2. Kudlik, G.; Takács, T.; Radnai, L.; Kurilla, A.; Szeder, B.; Koprivanacz, K.; Merő, B.L.; Buday, L.; Vas, V. Advances in Understanding TKS4 and TKS5: Molecular Scaffolds Regulating Cellular Processes from Podosome and Invadopodium Formation to Differentiation and Tissue Homeostasis. Int. J. Mol. Sci. 2020, 21, doi:10.3390/ijms21218117.
3. Courtneidge, S.A. Cell Migration and Incion in Human Disease: The Tks Adaptor Proteins. Biochem. Soc. Trans. 2012, 40, 129–132.
4. Maas, S.M.; Kayserili, H.; Lam, J.; Apak, M.Y.; Hennekam, R.C.M. Further Delineation of Frank-Ter Haar Syndrome. Am. J. Med. Genet. A 2004, 131, 127–133.
5. Gábor Bögel, Annamária Gujdár, Miklós Geiszt, Árpád Lányi, Anna Fekete, Szabolcs Sipeki, Julian Downward, László Buday Frank-Ter Haar Syndrome Protein Tks4 Regulates Epidermal Growth Factor-Dependent Cell Migration. J. Biol. Chem. 2012, 287, 31321–31329.
6. Durand, B.; Stoetzel, C.; Schaefer, E.; Calmels, N.; Scheidecker, S.; Kempf, N.; De Melo, C.; Guilbert, A.-S.; Timbolschi, D.; Donato, L.; et al. A Severe Case of Frank-Ter Haar Syndrome and Literature Review: Further Delineation of the Phenotypical Spectrum. Eur. J. Med. Genet. 2020, 63, 103857.
7. Iqbal, Z.; Cejudo-Martin, P.; de Brouwer, A.; van der Zwaag, B.; Ruiz-Lozano, P.; Scimia, M.C.; Lindsey, J.D.; Weinreb, R.; Albrecht, B.; Megarbane, A.; et al. Disruption of the Podosome Adaptor Protein TKS4 (SH3PXD2B) Causes the Skeletal Dysplasia, Eye, and Cardiac Abnormalities of Frank-Ter Haar Syndrome. Am. J. Hum. Genet. 2010, 86, 254–261.
8. Mao, M.; Thedens, D.R.; Chang, B.; Harris, B.S.; Zheng, Q.Y.; Johnson, K.R.; Donahue, L.R.; Anderson, M.G. The Podosomal-Adaptor Protein SH3PXD2B Is Essential for Normal Postnatal Development. Mamm. Genome 2009, 20, 462–475.
9. Szeder, B.; Tárnoki-Zách, J.; Lakatos, D.; Vas, V.; Kudlik, G.; Merő, B.; Koprivanacz, K.; Bányai, L.; Hámori, L.; Róna, G.; et al. Absence of the Tks4 Scaffold Protein Induces Epithelial-Mesenchymal Transition-Like Changes in Human Colon Cancer Cells. Cells 2019, 8, doi:10.3390/cells8111343.
10. Kurilla, A.; László, L.; Takács, T.; Tilajka, Á.; Lukács, L.; Novák, J.; Pancsa, R.; Buday, L.; Vas, V. Studying the Association of TKS4 and CD2AP Scaffold Proteins and Their Implications in the Partial Epithelial-Mesenchymal Transition (EMT) Process. Int. J. Mol. Sci. 2023, 24, doi:10.3390/ijms242015136.
11. László, L.; Maczelka, H.; Takács, T.; Kurilla, A.; Tilajka, Á.; Buday, L.; Vas, V.; Apáti, Á. A Novel Cell-Based Model for a Rare Disease: The Tks4-KO Human Embryonic Stem Cell Line as a Frank-Ter Haar Syndrome Model System. Int. J. Mol. Sci. 2022, 23, 8803.
12. Dülk, M.; Szeder, B.; Glatz, G.; Merő, B.L.; Koprivanacz, K.; Kudlik, G.; Vas, V.; Sipeki, S.; Cserkaszky, A.; Radnai, L.; et al. EGF Regulates the Interaction of Tks4 with Src through Its SH2 and SH3 Domains. Biochemistry 2018, 57, 4186–4196.
13. Müller, J. Transcriptional Silencing by the Polycomb Protein in Drosophila Embryos. EMBO J. 1995, 14, 1209–1220.
14. Margueron, R.; Reinberg, D. The Polycomb Complex PRC2 and Its Mark in Life. Nature 2011, 469, doi:10.1038/nature09784.
15. Lavelle, C.; Victor, J.-M. Nuclear Architecture and Dynamics; Academic Press, 2017; ISBN 9780128035030.
16. Schoenfelder, S.; Sugar, R.; Dimond, A.; Javierre, B.-M.; Armstrong, H.; Mifsud, B.; Dimitrova, E.; Matheson, L.; Tavares-Cadete, F.; Furlan-Magaril, M.; et al. Polycomb Repressive Complex PRC1 Spatially Constrains the Mouse Embryonic Stem Cell Genome. Nat. Genet. 2015, 47, 1179–1186.
17. Kundu, S.; Ji, F.; Sunwoo, H.; Jain, G.; Lee, J.T.; Sadreyev, R.I.; Dekker, J.; Kingston, R.E. Polycomb Repressive Complex 1 Generates Discrete Compacted Domains That Change during Differentiation. Mol. Cell 2017, 65, 432–446.e5.
18. Schuettengruber, B.; Cavalli, G. Recruitment of Polycomb Group Complexes and Their Role in the Dynamic Regulation of Cell Fate Choice. Development 2009, 136, 3531–3542.

 doi:10.20944/preprints202403.0787.v1




19. Kaneko, S.; Li, G.; Son, J.; Xu, C.-F.; Margueron, R.; Neubert, T.A.; Reinberg, D. Phosphorylation of the PRC2 Component Ezh2 Is Cell Cycle-Regulated and up-Regulates Its Binding to ncRNA. Genes Dev. 2010, 24, 2615–2620.
20. Nakagawa, M.; Kitabayashi, I. Oncogenic Roles of Enhancer of Zeste Homolog 1/2 in Hematological Malignancies. Cancer Sci. 2018, 109, 2342–2348.
21. Hosogane, M.; Funayama, R.; Shirota, M.; Nakayama, K. Lack of Transcription Triggers H3K27me3 Accumulation in the Gene Body. Cell Rep. 2016, 16, 696–706.
22. Bernstein, B.E.; Mikkelsen, T.S.; Xie, X.; Kamal, M.; Huebert, D.J.; Cuff, J.; Fry, B.; Meissner, A.; Wernig, M.; Plath, K.; et al. A Bivalent Chromatin Structure Marks Key Developmental Genes in Embryonic Stem Cells. Cell 2006, 125, 315–326.
23. Zhang, Z.; Wang, X.; Kim, M.; He, D.; Wang, C.; Fong, K.W.; Liu, X. Downregulation of EZH2 Inhibits Epithelial-Mesenchymal Transition in Enzalutamide-Resistant Prostate Cancer. Prostate 2023, 83, 1458–1469.
24. Battistelli, C.; Cicchini, C.; Santangelo, L.; Tramontano, A.; Grassi, L.; Gonzalez, F.J.; de Nonno, V.; Grassi, G.; Amicone, L.; Tripodi, M. The Snail Repressor Recruits EZH2 to Specific Genomic Sites through the Enrollment of the lncRNA HOTAIR in Epithelial-to-Mesenchymal Transition. Oncogene 2016, 36, 942–955.
25. Zhou, X.; Chen, H.; Hu, Y.; Ma, X.; Li, J.; Shi, Y.; Tao, M.; Wang, Y.; Zhong, Q.; Yan, D.; et al. Enhancer of Zeste Homolog 2 Promotes Renal Fibrosis after Acute Kidney Injury by Inducing Epithelial-Mesenchymal Transition and Activation of M2 Macrophage Polarization. Cell Death Dis. 2023, 14, 253.
26. Ghobashi, A.H.; Vuong, T.T.; Kimani, J.W.; Ladaika, C.A.; Hollenhorst, P.C.; O'Hagan, H.M. Activation of AKT Induces EZH2-Mediated β-Catenin Trimethylation in Colorectal Cancer. iScience 2023, 26, 107630.
27. Ardalan Khales, S.; Forghanifard, M.M.; Abbaszadegan, M.R.; Hosseini, S.E. EZH2 Deregulates BMP, Hedgehog, and Hippo Cell Signaling Pathways in Esophageal Squamous Cell Carcinoma. Adv. Med. Sci. 2023, 68, 21–30.
28. Sreeshma, B.; Devi, A. JARID2 and EZH2, the Eminent Epigenetic Drivers in Human Cancer. Gene 2023, 879, 147584.
29. Liu, J.; Fan, H.; Liang, X.; Chen, Y. Polycomb Repressor Complex: Its Function in Human Cancer and Therapeutic Target Strategy. Biomed. Pharmacother. 2023, 169, 115897.
30. Liu, Y.; Yang, Q. The Roles of EZH2 in Cancer and Its Inhibitors. Med. Oncol. 2023, 40, 167.
31. Yang, X.; Xu, L.; Yang, L. Recent Advances in EZH2-Based Dual Inhibitors in the Treatment of Cancers. Eur. J. Med. Chem. 2023, 256, 115461.
32. Hashemi, M.; Nazdari, N.; Gholamiyan, G.; Paskeh, M.D.A.; Jafari, A.M.; Nemati, F.; Khodaei, E.; Abyari, G.; Behdadfar, N.; Raei, B.; et al. EZH2 as a Potential Therapeutic Target for Gastrointestinal Cancers. Pathol. Res. Pract. 2024, 253, 154988.
33. Jacksi, M.; Schad, E.; Buday, L.; Tantos, A. Absence of Scaffold Protein Tks4 Disrupts Several Signaling Pathways in Colon Cancer Cells. Int. J. Mol. Sci. 2023, 24, doi:10.3390/ijms24021310.
34. Kim, D.; Paggi, J.M.; Park, C.; Bennett, C.; Salzberg, S.L. Graph-Based Genome Alignment and Genotyping with HISAT2 and HISAT-Genotype. Nat. Biotechnol. 2019, 37, 907–915.
35. Li, H.; Handsaker, B.; Wysoker, A.; Fennell, T.; Ruan, J.; Homer, N.; Marth, G.; Abecasis, G.; Durbin, R.; 1000 Genome Project Data Processing Subgroup The Sequence Alignment/Map Format and SAMtools. Bioinformatics 2009, 25, 2078–2079.
36. Trapnell, C.; Roberts, A.; Goff, L.; Pertea, G.; Kim, D.; Kelley, D.R.; Pimentel, H.; Salzberg, S.L.; Rinn, J.L.; Pachter, L. Differential Gene and Transcript Expression Analysis of RNA-Seq Experiments with TopHat and Cufflinks. Nat. Protoc. 2012, 7, 562–578.
37. Kelley, L.G.C.T. cummeRbund; Bioconductor, 2017;.
38. Schneider, C.A.; Rasband, W.S.; Eliceiri, K.W. NIH Image to ImageJ: 25 Years of Image Analysis. Nat. Methods 2012, 9, 671–675.
39. Katona, B.W.; Liu, Y.; Ma, A.; Jin, J.; Hua, X. EZH2 Inhibition Enhances the Efficacy of an EGFR Inhibitor in Suppressing Colon Cancer Cells. Cancer Biol. Ther. 2014, 15, 1677–1687.
40. Gall, T.M.H.; Frampton, A.E. Gene of the Month: E-Cadherin (CDH1). J. Clin. Pathol. 2013, 66, 928–932.
41. Overgaard, C.E.; Mitchell, L.A.; Koval, M. Roles for Claudins in Alveolar Epithelial Barrier Function. Ann. N. Y. Acad. Sci. 2012, 1257, 167–174.

 doi:10.20944/preprints202403.0787.v1




42. Conceição, A.L.G.; Da Silva, C.T.; Badial, R.M.; Valsechi, M.C.; Stuqui, B.; Gonçalves, J.D.; Jasiulionis, M.G.; De Freitas Calmon, M.; Rahal, P. Downregulation of OCLN and GAS1 in Clear Cell Renal Cell Carcinoma. Oncol. Rep. 2017, 37, 1487–1496.
43. Riz, I.; Hawley, R.G. Increased Expression of the Tight Junction Protein TJP1/ZO-1 Is Associated with Upregulation of TAZ-TEAD Activity and an Adult Tissue Stem Cell Signature in Carfilzomib-Resistant Multiple Myeloma Cells and High-Risk Multiple Myeloma Patients. Oncoscience 2017, 4, 79.
44. Diversity of Cytokeratins: Differentiation Specific Expression of Cytokeratin Polypeptides in Epithelial Cells and Tissues. J. Mol. Biol. 1981, 153, 933–959.
45. Yang, Y.; Zhang, N.; Zhu, J.; Hong, X.-T.; Liu, H.; Ou, Y.-R.; Su, F.; Wang, R.; Li, Y.-M.; Wu, Q. Downregulated connexin32 Promotes EMT through the Wnt/β-Catenin Pathway by Targeting Snail Expression in Hepatocellular Carcinoma. Int. J. Oncol. 2017, 50, 1977–1988.
46. Connexins, Gap Junctions and Tissue Invasion. FEBS Lett. 2014, 588, 1331–1338.
47. Sudo, T.; Iwaya, T.; Nishida, N.; Sawada, G.; Takahashi, Y.; Ishibashi, M.; Shibata, K.; Fujita, H.; Shirouzu, K.; Mori, M.; et al. Expression of Mesenchymal Markers Vimentin and Fibronectin: The Clinical Significance in Esophageal Squamous Cell Carcinoma. Ann. Surg. Oncol. 2012, 20, 324–335.
48. Leader, M.; Collins, M.; Patel, J.; Henry, K. Vimentin: An Evaluation of Its Role as a Tumour Marker. Histopathology 1987, 11, 63–72.
49. Usami, Y.; Satake, S.; Nakayama, F.; Matsumoto, M.; Ohnuma, K.; Komori, T.; Semba, S.; Ito, A.; Yokozaki, H. Snail-Associated Epithelial–mesenchymal Transition Promotes Oesophageal Squamous Cell Carcinoma Motility and Progression. J. Pathol. 2008, 215, 330–339.
50. Steinbichler, T.B.; Dudas, J.; Ingruber, J.; Glueckert, R.; Sprung, S.; Fleischer, F.; Cidlinsky, N.; Dejaco, D.; Kofler, B.; Giotakis, A.I.; et al. Slug Is A Surrogate Marker of Epithelial to Mesenchymal Transition (EMT) in Head and Neck Cancer. J. Clin. Med. Res. 2020, 9, 2061.
51. Pozharskaya, V.; Torres-González, E.; Rojas, M.; Gal, A.; Amin, M.; Dollard, S.; Roman, J.; Stecenko, A.A.; Mora, A.L. Twist: A Regulator of Epithelial-Mesenchymal Transition in Lung Fibrosis. PLoS One 2009, 4, e7559.
52. Larsen, J.E.; Nathan, V.; Osborne, J.K.; Farrow, R.K.; Deb, D.; Sullivan, J.P.; Dospoy, P.D.; Augustyn, A.; Hight, S.K.; Sato, M.; et al. ZEB1 Drives Epithelial-to-Mesenchymal Transition in Lung Cancer. J. Clin. Invest. 2016, 126, 3219–3235.
53. Vilorio-Marqués, L.; Martín, V.; Diez-Tascón, C.; González-Sevilla, M.F.; Fernández-Villa, T.; Honrado, E.; Davila-Batista, V.; Molina, A.J. The Role of EZH2 in Overall Survival of Colorectal Cancer: A Meta-Analysis. Sci. Rep. 2017, 7, 13806.
54. Mahmood, N.; Mihalcioiu, C.; Rabbani, S.A. Multifaceted Role of the Urokinase-Type Plasminogen Activator (uPA) and Its Receptor (uPAR): Diagnostic, Prognostic, and Therapeutic Applications. Front. Oncol. 2018, 8, 24.
55. Miyazaki, K. Laminin-5 (laminin-332): Unique Biological Activity and Role in Tumor Growth and Invasion. Cancer Sci. 2006, 97, 91–98.
56. Caley, M.P.; Martins, V.L.; Moore, K.; Lashari, M.; Nissinen, L.; Kähäri, V.-M.; Alexander, S.; Jones, E.; Harwood, C.A.; Jones, J.; et al. Loss of the Laminin Subunit Alpha-3 Induces Cell Invasion and Macrophage Infiltration in Cutaneous Squamous Cell Carcinoma. Br. J. Dermatol. 2021, 184, 923–934.
57. Patarroyo, M.; Tryggvason, K.; Virtanen, I. Laminin Isoforms in Tumor Invasion, Angiogenesis and Metastasis. Semin. Cancer Biol. 2002, 12, 197–207.
58. Sun, S.; Wang, Y.; Wu, Y.; Gao, Y.; Li, Q.; Abdulrahman, A.A.; Liu, X.-F.; Ji, G.-Q.; Gao, J.; Li, L.; et al. Identification of COL1A1 as an Invasion-related Gene in Malignant Astrocytoma. Int. J. Oncol. 2018, 53, 2542–2554.
59. Pasco, S.; Brassart, B.; Ramont, L.; Maquart, F.-X.; Monboisse, J.-C. Control of Melanoma Cell Invasion by Type IV Collagen. Cancer Detect. Prev. 2005, 29, 260–266.
60. Tian, X.; Sun, J.; Li, C.; Zhang, K. COL4A1 Promotes the Proliferation and Migration of Oral Squamous Cell Carcinoma Cells by Binding to NID1. Exp. Ther. Med. 2023, 25, 176.
61. Owusu-Ansah, K.G.; Song, G.; Chen, R.; Edoo, M.I.A.; Li, J.; Chen, B.; Wu, J.; Zhou, L.; Xie, H.; Jiang, D.; et al. COL6A1 Promotes Metastasis and Predicts Poor Prognosis in Patients with Pancreatic Cancer. Int. J. Oncol. 2019, 55, 391–404.

62. Ni, S.; Weng, W.; Xu, M.; Wang, Q.; Tan, C.; Sun, H.; Wang, L.; Huang, D.; Du, X.; Sheng, W. miR-106b-5p Inhibits the Invasion and Metastasis of Colorectal Cancer by Targeting CTSA. Onco. Targets. Ther. 2018, 11, 3835–3845.
63. Park, S.; Kwon, W.; Park, J.-K.; Baek, S.-M.; Lee, S.-W.; Cho, G.-J.; Ha, Y.-S.; Lee, J.N.; Kwon, T.G.; Kim, M.O.; et al. Suppression of Cathepsin a Inhibits Growth, Migration, and Invasion by Inhibiting the p38 MAPK Signaling Pathway in Prostate Cancer. Arch. Biochem. Biophys. 2020, 688, 108407.
64. Ruan, J.; Zheng, H.; Rong, X.; Rong, X.; Zhang, J.; Fang, W.; Zhao, P.; Luo, R. Over-Expression of Cathepsin B in Hepatocellular Carcinomas Predicts Poor Prognosis of HCC Patients. Mol. Cancer 2016, 15, 17.
65. Harbeck, N.; Thomssen, C.; Berger, U.; Ulm, K.; Kates, R.E.; Höfler, H.; Jänicke, F.; Graeff, H.; Schmitt, M. Invasion Marker PAI-1 Remains a Strong Prognostic Factor after Long-term Follow-up Both for Primary Breast Cancer and Following First Relapse. Breast Cancer Res. Treat. 1999, 54, 147–157.
66. Westermarck, J.; Kähäri, V.M. Regulation of Matrix Metalloproteinase Expression in Tumor Invasion. FASEB J. 1999, 13.
67. Shiomi, T.; Okada, Y. MT1-MMP and MMP-7 in Invasion and Metastasis of Human Cancers. Cancer Metastasis Rev. 2003, 22, 145–152.
68. Wang, X.; Lu, H.; Urvalek, A.M.; Li, T.; Yu, L.; Lamar, J.; DiPersio, C.M.; Feustel, P.J.; Zhao, J. KLF8 Promotes Human Breast Cancer Cell Invasion and Metastasis by Transcriptional Activation of MMP9. Oncogene 2011, 30, 1901–1911.
69. Ala-Aho, R.; Johansson, N.; Baker, A.H.; Kähäri, V.-M. Expression of Collagenase-3 (MMP-13) Enhances Invasion of Human Fibrosarcoma HT-1080 Cells. Int. J. Cancer 2002, 97, 283–289.
70. Yan, T.; Lin, Z.; Jiang, J.; Lu, S.; Chen, M.; Que, H.; He, X.; Que, G.; Mao, J.; Xiao, J.; et al. MMP14 Regulates Cell Migration and Invasion through Epithelial-Mesenchymal Transition in Nasopharyngeal Carcinoma. Am. J. Transl. Res. 2015, 7, 950–958.
71. Huang, W.; Zhu, J.; Shi, H.; Wu, Q.; Zhang, C. ITGA2 Overexpression Promotes Esophageal Squamous Cell Carcinoma Aggression via FAK/AKT Signaling Pathway. Onco. Targets. Ther. 2021, 14, 3583–3596.
72. Tian, L.; Chen, M.; He, Q.; Yan, Q.; Zhai, C. MicroRNA-199a-5p Suppresses Cell Proliferation, Migration and Invasion by Targeting ITGA3 in Colorectal Cancer. Mol. Med. Rep. 2020, 22, 2307–2317.
73. Li, X.-L.; Liu, L.; Li, D.-D.; He, Y.-P.; Guo, L.-H.; Sun, L.-P.; Liu, L.-N.; Xu, H.-X.; Zhang, X.-P. Integrin β4 Promotes Cell Invasion and Epithelial-Mesenchymal Transition through the Modulation of Slug Expression in Hepatocellular Carcinoma. Sci. Rep. 2017, 7, 40464.
74. Sun, X.; Kaufman, P.D. Ki-67: More than a Proliferation Marker. Chromosoma 2018, 127, 175–186.
75. Liu, P.; Kao, T.P.; Huang, H. CDK1 Promotes Cell Proliferation and Survival via Phosphorylation and Inhibition of FOXO1 Transcription Factor. Oncogene 2008, 27, 4733–4744.
76. Fiaschi-Taesch, N.M.; Salim, F.; Kleinberger, J.; Troxell, R.; Cozar-Castellano, I.; Selk, K.; Cherok, E.; Takane, K.K.; Scott, D.K.; Stewart, A.F. Induction of Human β-Cell Proliferation and Engraftment Using a Single G1/S Regulatory Molecule, cdk6. Diabetes 2010, 59, 1926–1936.
77. Upregulation of CDK7 in Gastric Cancer Cell Promotes Tumor Cell Proliferation and Predicts Poor Prognosis. Exp. Mol. Pathol. 2016, 100, 514–521.
78. Li, X.-Y.; Luo, Q.-F.; Wei, C.-K.; Li, D.-F.; Fang, L. siRNA-Mediated Silencing of CDK8 Inhibits Proliferation and Growth in Breast Cancer Cells. Int. J. Clin. Exp. Pathol. 2014, 7, 92.
79. Porter, L.A.; Dellinger, R.W.; Tynan, J.A.; Barnes, E.A.; Kong, M.; Lenormand, J.-L.; Donoghue, D.J. Human Speedy a Novel Cell Cycle Regulator That Enhances Proliferation through Activation of Cdk2. J. Cell Biol. 2002, 157, 357–366.
80. Ma, Q. MiR-219-5p Suppresses Cell Proliferation and Cell Cycle Progression in Esophageal Squamous Cell Carcinoma by Targeting CCNA2. Cell. Mol. Biol. Lett. 2019, 24, 1–13.
81. Lew, D.J.; Reed, S.I. A Proliferation of Cyclins. Trends Cell Biol. 1992, 2, 77–81.
82. Cooper, S. Cyclin D1 Serves as a Cell Cycle Regulatory Switch in Actively Proliferating Cells. Curr. Opin. Cell Biol. 2003, 15, 158–163.
83. Cyclin-Dependent Kinase Inhibitors. Curr. Opin. Pharmacol. 2003, 3, 362–370.
84. Manohar, S.M.; Joshi, K.S. Molecular Pharmacology of Multitarget Cyclin-Dependent Kinase Inhibitors in Human Colorectal Carcinoma Cells. Expert Opin. Ther. Targets 2023, doi:10.1080/14728222.2023.2199924.
85. Andrés-Sánchez, N.; Fisher, D.; Krasinska, L. Physiological Functions and Roles in Cancer of the Proliferation Marker Ki-67. J. Cell Sci. 2022, 135, doi:10.1242/jcs.258932.

86. Passardi, A.; Gibbons, D. Molecular Targets for the Treatment of Metastatic Colorectal Cancer; Frontiers Media SA, 2024; ISBN 9782832542064.
87. O'Leary, B.; Finn, R.S.; Turner, N.C. Treating Cancer with Selective CDK4/6 Inhibitors. Nat. Rev. Clin. Oncol. 2016, 13, 417–430.
88. Lehtonen, S.; Ryan, J.J.; Kudlicka, K.; Iino, N.; Zhou, H.; Farquhar, M.G. Cell Junction-Associated Proteins IQGAP1, MAGI-2, CASK, Spectrins, and Alpha-Actinin Are Components of the Nephrin Multiprotein Complex. Proc. Natl. Acad. Sci. U. S. A. 2005, 102, 9814–9819.
89. Tong, J.; Han, C.-J.; Zhang, J.-Z.; He, W.-Z.; Zhao, G.-J.; Cheng, X.; Zhang, L.; Deng, K.-Q.; Liu, Y.; Fan, H.-F.; et al. Hepatic Interferon Regulatory Factor 6 Alleviates Liver Steatosis and Metabolic Disorder by Transcriptionally Suppressing Peroxisome Proliferator-Activated Receptor γ in Mice. Hepatology 2019, 69, 2471–2488.
90. Raschperger, E. Studies on CAR and CLMP : Two Proteins of Epithelial Tight Junctions, Institutionen för cell- och molekylärbiologi (CMB) / Department of Cell and Molecular Biology, 2006.
91. Kimura-Yoshida, C.; Mochida, K.; Nakaya, M.-A.; Mizutani, T.; Matsuo, I. Cytoplasmic Localization of GRHL3 upon Epidermal Differentiation Triggers Cell Shape Change for Epithelial Morphogenesis. Nat. Commun. 2018, 9, 1–17.
92. Cech, T.R.; Steitz, J.A. The Noncoding RNA Revolution-Trashing Old Rules to Forge New Ones. Cell 2014, 157, 77–94.
93. Mattick, J.S.; Amaral, P.P.; Carninci, P.; Carpenter, S.; Chang, H.Y.; Chen, L.-L.; Chen, R.; Dean, C.; Dinger, M.E.; Fitzgerald, K.A.; et al. Long Non-Coding RNAs: Definitions, Functions, Challenges and Recommendations. Nat. Rev. Mol. Cell Biol. 2023, 24, 430–447.
94. Snyder, M.; Iraola-Guzmán, S.; Saus, E.; Gabaldón, T. Discovery and Validation of Clinically Relevant Long Non-Coding RNAs in Colorectal Cancer. Cancers 2022, 14, doi:10.3390/cancers14163866.
95. Aprile, M.; Costa, V.; Cimmino, A.; Calin, G.A. Emerging Role of Oncogenic Long Non-Coding RNA as Cancer Biomarkers. Int. J. Cancer 2022, doi:10.1002/ijc.34282.
96. Gupta, R.A.; Shah, N.; Wang, K.C.; Kim, J.; Horlings, H.M.; Wong, D.J.; Tsai, M.-C.; Hung, T.; Argani, P.; Rinn, J.L.; et al. Long Non-Coding RNA HOTAIR Reprograms Chromatin State to Promote Cancer Metastasis. Nature 2010, 464, 1071–1076.
97. Ma, D.N.; Chai, Z.T.; Zhu, X.D.; Zhang, N.; Zhan, D.H.; Ye, B.G.; Wang, C.H.; Qin, C.D.; Zhao, Y.M.; Zhu, W.P.; et al. MicroRNA-26a Suppresses Epithelial-Mesenchymal Transition in Human Hepatocellular Carcinoma by Repressing Enhancer of Zeste Homolog 2. J. Hematol. Oncol. 2016, 9, doi:10.1186/s13045-015-0229-y.
98. Cao, Q.; Yu, J.; Dhanasekaran, S.M.; Kim, J.H.; Mani, R.S.; Tomlins, S.A.; Mehra, R.; Laxman, B.; Cao, X.; Yu, J.; et al. Repression of E-Cadherin by the Polycomb Group Protein EZH2 in Cancer. Oncogene 2008, 27, doi:10.1038/onc.2008.333.
99. Wang, J.; Zhu, X.; Hu, J.; He, G.; Li, X.; Wu, P.; Ren, X.; Wang, F.; Liao, W.; Liang, L.; et al. The Positive Feedback between Snail and DAB2IP Regulates EMT, Invasion and Metastasis in Colorectal Cancer. Oncotarget 2015, 6, doi:10.18632/oncotarget.4861.
100. Yi, X.; Guo, J.; Guo, J.; Sun, S.; Yang, P.; Wang, J.; Li, Y.; Xie, L.; Cai, J.; Wang, Z. EZH2-Mediated Epigenetic Silencing of TIMP2 Promotes Ovarian Cancer Migration and Invasion. Sci. Rep. 2017, 7, 3568.
101. Chien, Y.-C.; Liu, L.-C.; Ye, H.-Y.; Wu, J.-Y.; Yu, Y.-L. EZH2 Promotes Migration and Invasion of Triple-Negative Breast Cancer Cells via Regulating TIMP2-MMP-2/-9 Pathway. Am. J. Cancer Res. 2018, 8, 422.
102. Rao, Z.-Y.; Cai, M.-Y.; Yang, G.-F.; He, L.-R.; Mai, S.-J.; Hua, W.-F.; Liao, Y.-J.; Deng, H.-X.; Chen, Y.-C.; Guan, X.-Y.; et al. EZH2 Supports Ovarian Carcinoma Cell Invasion And/or Metastasis via Regulation of TGF-β1 and Is a Predictor of Outcome in Ovarian Carcinoma Patients. Carcinogenesis 2010, 31, 1576–1583.
103. Stölting, M.; Wiesner, C.; van Vliet, V.; Butt, E.; Pavenstädt, H.; Linder, S.; Kremerskothen, J. Lasp-1 Regulates Podosome Function. PLoS One 2012, 7, e35340.
104. Buccione, R.; Orth, J.D.; McNiven, M.A. Foot and Mouth: Podosomes, Invadopodia and Circular Dorsal Ruffles. Nat. Rev. Mol. Cell Biol. 2004, 5, 647–657.
105. Mitre, G.P.; Balbinot, K.M.; Ribeiro, A.L.R.; da Silva Kataoka, M.S.; de Melo Alves Júnior, S.; de Jesus Viana Pinheiro, J. Key Proteins of Invadopodia Are Overexpressed in Oral Squamous Cell Carcinoma Suggesting an Important Role of MT1-MMP in the Tumoral Progression. Diagn. Pathol. 2021, 16, 33.
106. Gimona, M.; Buccione, R.; Courtneidge, S.A.; Linder, S. Assembly and Biological Role of Podosomes and Invadopodia. Current Opinion in Cell Biology 2008, 20, 235–241.

107. Iizuka, S.; Abdullah, C.; Buschman, M.D.; Diaz, B.; Courtneidge, S.A. The Role of Tks Adaptor Proteins in Invadopodia Formation, Growth and Metastasis of Melanoma. Oncotarget 2016, 7, 78473.
108. Zhao, H.; Ming, T.; Tang, S.; Ren, S.; Yang, H.; Liu, M.; Tao, Q.; Xu, H. Wnt Signaling in Colorectal Cancer: Pathogenic Role and Therapeutic Target. Mol. Cancer 2022, 21, 144.
109. Noorolyai, S.; Shajari, N.; Baghbani, E.; Sadreddini, S.; Baradaran, B. The Relation between PI3K/AKT Signalling Pathway and Cancer. Gene 2019, 698, doi:10.1016/j.gene.2019.02.076.
110. Wilkins-Port, C.E.; Ye, Q.; Mazurkiewicz, J.E.; Higgins, P.J. TGF-beta1 + EGF-Initiated Invasive Potential in Transformed Human Keratinocytes Is Coupled to a plasmin/MMP-10/MMP-1-Dependent Collagen Remodeling Axis: Role for PAI-1. Cancer Res. 2009, 69, 4081–4091.
111. Pavón, M.A.; Arroyo-Solera, I.; Téllez-Gabriel, M.; León, X.; Virós, D.; López, M.; Gallardo, A.; Céspedes, M.V.; Casanova, I.; López-Pousa, A.; et al. Enhanced Cell Migration and Apoptosis Resistance May Underlie the Association between High SERPINE1 Expression and Poor Outcome in Head and Neck Carcinoma Patients. Oncotarget 2015, 6, 29016–29033.
112. Buikhuisen, J.Y.; Gomez Barila, P.M.; Torang, A.; Dekker, D.; de Jong, J.H.; Cameron, K.; Vitale, S.; Stassi, G.; van Hooff, S.R.; Castro, M.A.A.; et al. AKT3 Expression in Mesenchymal Colorectal Cancer Cells Drives Growth and Is Associated with Epithelial-Mesenchymal Transition. Cancers 2021, 13, doi:10.3390/cancers13040801.
113. He, S.; Liu, Y.; Meng, L.; Sun, H.; Wang, Y.; Ji, Y.; Purushe, J.; Chen, P.; Li, C.; Madzo, J.; et al. Ezh2 Phosphorylation State Determines Its Capacity to Maintain CD8 T Memory Precursors for Antitumor Immunity. Nat. Commun. 2017, 8, 2125.
114. Kikuchi, J.; Koyama, D.; Wada, T.; Izumi, T.; Hofgaard, P.O.; Bogen, B.; Furukawa, Y. Phosphorylation-Mediated EZH2 Inactivation Promotes Drug Resistance in Multiple Myeloma. J. Clin. Invest. 2015, 125, 4375–4390.
115. Yamada, L.; Saito, M.; Thar Min, A.K.; Saito, K.; Ashizawa, M.; Kase, K.; Nakajima, S.; Onozawa, H.; Okayama, H.; Endo, H.; et al. Selective Sensitivity of EZH2 Inhibitors Based on Synthetic Lethality in ARID1A-Deficient Gastric Cancer. Gastric Cancer 2021, 24, 60–71.
116. Yi, C.; Li, G.; Wang, W.; Sun, Y.; Zhang, Y.; Zhong, C.; Stovall, D.B.; Li, D.; Shi, J.; Sui, G. Disruption of YY1-EZH2 Interaction Using Synthetic Peptides Inhibits Breast Cancer Development. Cancers 2021, 13, doi:10.3390/cancers13102402.
117. Kosalai, S.T.; Morsy, M.H.A.; Papakonstantinou, N.; Mansouri, L.; Stavroyianni, N.; Kanduri, C.; Stamatopoulos, K.; Rosenquist, R.; Kanduri, M. EZH2 Upregulates the PI3K/AKT Pathway through IGF1R and MYC in Clinically Aggressive Chronic Lymphocytic Leukaemia. Epigenetics 2019, 14, 1125–1140.
118. Ferraro, A.; Mourtzoukou, D.; Kosmidou, V.; Avlonitis, S.; Kontogeorgos, G.; Zografos, G.; Pintzas, A. EZH2 Is Regulated by ERK/AKT and Targets Integrin alpha2 Gene to Control Epithelial-Mesenchymal Transition and Anoikis in Colon Cancer Cells. Int. J. Biochem. Cell Biol. 2013, 45, 243–254.
119. Feng, H.; Yu, Z.; Tian, Y.; Lee, Y.-Y.; Li, M.S.; Go, M.Y.Y.; Cheung, Y.-S.; Lai, P.B.S.; Chan, A.M.L.; To, K.-F.; et al. A CCRK-EZH2 Epigenetic Circuitry Drives Hepatocarcinogenesis and Associates with Tumor Recurrence and Poor Survival of Patients. J. Hepatol. 2015, 62, 1100–1111.
120. Rawlings, J.S.; Rosler, K.M.; Harrison, D.A. The JAK/STAT Signaling Pathway. J. Cell Sci. 2004, 117, 1281–1283.
121. Chen, X.; Hao, A.; Li, X.; Du, Z.; Li, H.; Wang, H.; Yang, H.; Fang, Z. Melatonin Inhibits Tumorigenicity of Glioblastoma Stem-like Cells via the AKT-EZH2-STAT3 Signaling Axis. J. Pineal Res. 2016, 61, 208–217.
122. Chen, B.; Liu, J.; Chang, Q.; Beezhold, K.; Lu, Y.; Chen, F. JNK and STAT3 Signaling Pathways Converge on Akt-Mediated Phosphorylation of EZH2 in Bronchial Epithelial Cells Induced by Arsenic. Cell Cycle 2013, 12, 112–121.
123. Biswas, R.; Bagchi, A. NFkB Pathway and Inhibition: An Overview. Computational Molecular Biology 2016, 6.
124. The Nuclear Factor Kappa B (NF-kB) Signaling in Cancer Development and Immune Diseases. Genes & Diseases 2021, 8, 287–297.
125. Min, J.; Zaslavsky, A.; Fedele, G.; McLaughlin, S.K.; Reczek, E.E.; De Raedt, T.; Guney, I.; Strochlic, D.E.; MacConaill, L.E.; Beroukhim, R.; et al. An Oncogene–tumor Suppressor Cascade Drives Metastatic Prostate Cancer by Coordinately Activating Ras and Nuclear Factor-κB. Nat. Med. 2010, 16, 286–294.
126. Waldner, M.J.; Neurath, M.F. Targeting the VEGF Signaling Pathway in Cancer Therapy. Expert Opin. Ther. Targets 2012, doi:10.1517/14728222.2011.641951.

 doi:10.20944/preprints202403.0787.v1




127. Xu, Z.Q.; Zhang, L.; Gao, B.S.; Wan, Y.G.; Zhang, X.H.; Chen, B.; Wang, Y.T.; Sun, N.; Fu, Y.W. EZH2 Promotes Tumor Progression by Increasing VEGF Expression in Clear Cell Renal Cell Carcinoma. Clin. Transl. Oncol. 2014, 17, 41–49.
128. Chen, Y.-T.; Zhu, F.; Lin, W.-R.; Ying, R.-B.; Yang, Y.-P.; Zeng, L.-H. The Novel EZH2 Inhibitor, GSK126, Suppresses Cell Migration and Angiogenesis via down-Regulating VEGF-A. Cancer Chemother. Pharmacol. 2016, 77, 757–765.
129. Riquelme, E.; Suraokar, M.; Behrens, C.; Lin, H.Y.; Girard, L.; Nilsson, M.B.; Simon, G.; Wang, J.; Coombes, K.R.; Lee, J.J.; et al. VEGF/VEGFR-2 Upregulates EZH2 Expression in Lung Adenocarcinoma Cells and EZH2 Depletion Enhances the Response to Platinum-Based and VEGFR-2–Targeted Therapy. Clin. Cancer Res. 2014, 20, 3849–3861.
130. Zhao, M.; Hu, X.; Xu, Y.; Wu, C.; Chen, J.; Ren, Y.; Kong, L.; Sun, S.; Zhang, L.; Jin, R.; et al. Targeting of EZH2 Inhibits Epithelial-mesenchymal Transition in Head and Neck Squamous Cell Carcinoma via Regulating the STAT3/VEGFR2 Axis. Int. J. Oncol. 2019, 55, 1165–1175.
131. Zou, Z.; Tao, T.; Li, H.; Zhu, X. mTOR Signaling Pathway and mTOR Inhibitors in Cancer: Progress and Challenges. Cell Biosci. 2020, 10, 1–11.
132. Yang, R.; Wang, M.; Zhang, G.; Bao, Y.; Wu, Y.; Li, X.; Yang, W.; Cui, H. E2F7-EZH2 Axis Regulates PTEN/AKT/mTOR Signalling and Glioblastoma Progression. Br. J. Cancer 2020, 123, 1445–1455.
133. Zheng, X.; Tsou, P.; Sawalha, A.H. Increased Expression of EZH2 Is Mediated by Higher Glycolysis and mTORC1 Activation in Lupus CD4+ T Cells. Immunometabolism 2020, 2, e200013.
134. Jarome, T.J.; Perez, G.A.; Hauser, R.M.; Hatch, K.M.; Lubin, F.D. EZH2 Methyltransferase Activity Controls Pten Expression and mTOR Signaling during Fear Memory Reconsolidation. J. Neurosci. 2018, 38, 7635–7648.
135. Fan, Y.; Shen, B.; Tan, M.; Mu, X.; Qin, Y.; Zhang, F.; Liu, Y. TGF-β–Induced Upregulation of malat1 Promotes Bladder Cancer Metastasis by Associating with suz12. Clin. Cancer Res. 2014, 20, 1531–1541.
136. Chen, Q.; Zhu, C.; Jin, Y. The Oncogenic and Tumor Suppressive Functions of the Long Noncoding RNA MALAT1: An Emerging Controversy. Front. Genet. 2020, 11, 505991.
137. Wang, X.; Sehgal, L.; Jain, N.; Khashab, T.; Mathur, R.; Samaniego, F. LncRNA MALAT1 Promotes Development of Mantle Cell Lymphoma by Associating with EZH2. J. Transl. Med. 2016, 14, 1–14.
138. Chen, M.; Xia, Z.; Chen, C.; Hu, W.; Yuan, Y. LncRNA MALAT1 Promotes Epithelial-to-Mesenchymal Transition of Esophageal Cancer through Ezh2-Notch1 Signaling Pathway. 2018, doi:10.1097/CAD.0000000000000645.
139. Wang, R.; Lu, X.; Yu, R. lncRNA MALAT1 Promotes EMT Process and Cisplatin Resistance of Oral Squamous Cell Carcinoma via PI3K/AKT/m-TOR Signal Pathway. Onco. Targets. Ther. 2020, 13, 4049–4061.
140. Zhang, K.; Sun, X.; Zhou, X.; Han, L.; Chen, L.; Shi, Z.; Zhang, A.; Ye, M.; Wang, Q.; Liu, C.; et al. Long Non-Coding RNA HOTAIR Promotes Glioblastoma Cell Cycle Progression in an EZH2 Dependent Manner. Oncotarget 2015, 6, 537.
141. Li, X.; Wu, Z.; Mei, Q.; Guo, M.; Fu, X.; Han, W. Long Non-Coding RNA HOTAIR, a Driver of Malignancy, Predicts Negative Prognosis and Exhibits Oncogenic Activity in Oesophageal Squamous Cell Carcinoma. Br. J. Cancer 2013, 109, 2266–2278.
142. Sadeghalvad, M.; Mansouri, K.; Mohammadi-Motlagh, H.-R.; Noorbakhsh, F.; Mostafaie, A.; Alipour, S.; Rezaei, N. Long Non-Coding RNA HOTAIR Induces the PI3K/AKT/mTOR Signaling Pathway in Breast Cancer Cells. Rev. Assoc. Med. Bras. 2022, 68, 456–462.
143. Zhang, C.; Li, J.-Y.; Tian, F.-Z.; Zhao, G.; Hu, H.; Ma, Y.-F.; Yang, Y.-L. Long Noncoding RNA NEAT1 Promotes Growth and Metastasis of Cholangiocarcinoma Cells. Oncol. Res. 2018, 26, 879–888.
144. Li, O.; Jiang, B.; Yi, W.-M.; Zhang, Y.; Yang, P.-Z.; Guo, C.; Sun, Z.-P.; Peng, C. LncRNA NEAT1 Promotes Cell Proliferation, Migration, and Invasion via the miR-186-5p/PTP4A1 Axis in Cholangiocarcinoma. Kaohsiung J. Med. Sci. 2021, 37, 379–391.
145. Chen, Q.; Cai, J.; Wang, Q.; Wang, Y.; Liu, M.; Yang, J.; Zhou, J.; Kang, C.; Li, M.; Jiang, C. Long Noncoding RNA , Regulated by the EGFR Pathway, Contributes to Glioblastoma Progression Through the WNT/-Catenin Pathway by Scaffolding EZH2. Clin. Cancer Res. 2018, 24, 684–695.
146. Wang, S.; Zuo, H.; Jin, J.; Lv, W.; Xu, Z.; Fan, Y.; Zhang, J.; Zuo, B. Long Noncoding RNA Neat1 Modulates Myogenesis by Recruiting Ezh2. Cell Death Dis. 2019, 10, 505.

147. Ge, Z.; Yin, C.; Li, Y.; Tian, D.; Xiang, Y.; Li, Q.; Tang, Y.; Zhang, Y. Long Noncoding RNA NEAT1 Promotes Cardiac Fibrosis in Heart Failure through Increased Recruitment of EZH2 to the Smad7 Promoter Region. J. Transl. Med. 2022, 20, 1–16.
148. Wang, Q.; Liu, L.; Zhang, S.; Ming, Y.; Liu, S.; Cheng, K.; Zhao, Y. Long Noncoding RNA NEAT1 Suppresses Hepatocyte Proliferation in Fulminant Hepatic Failure through Increased Recruitment of EZH2 to the LATS2 Promoter Region and Promotion of H3K27me3 Methylation. Exp. Mol. Med. 2020, 52, doi:10.1038/s12276-020-0387-z.
149. Wan, Y.; Yao, Z.; Chen, W.; Li, D. The lncRNA NORAD/miR-520a-3p Facilitates Malignancy in Non-Small Cell Lung Cancer via PI3k/Akt/mTOR Signaling Pathway. Onco. Targets. Ther. 2020, 13, 1533–1544.
150. Geng, Q.; Li, Z.; Li, X.; Wu, Y.; Chen, N. LncRNA NORAD, Sponging miR-363-3p, Promotes Invasion and EMT by Upregulating PEAK1 and Activating the ERK Signaling Pathway in NSCLC Cells. J. Bioenerg. Biomembr. 2021, 53, 321–332.
151. Zhang, Y.; Li, Y. Long Non-Coding RNA NORAD Contributes to the Proliferation, Invasion and EMT Progression of Prostate Cancer via the miR-30a-5p/RAB11A/WNT/β-Catenin Pathway. Cancer Cell Int. 2020, 20, 571.
152. Wu, G.; Su, J.; Zeng, L.; Deng, S.; Huang, X.; Ye, Y.; Li, R.; Bai, R.; Zhuang, L.; Li, M.; et al. LncRNA BCAN-AS1 Stabilizes c-Myc via N-Methyladenosine-Mediated Binding with SNIP1 to Promote Pancreatic Cancer. Cell Death Differ. 2023, 30, 2213–2230.
153. Gao, L.-F.; Li, W.; Liu, Y.-G.; Zhang, C.; Gao, W.-N.; Wang, L. Inhibition of MIR4435-2HG on Invasion, Migration, and EMT of Gastric Carcinoma Cells by Mediating MiR-138-5p/Sox4 Axis. Front. Oncol. 2021, 11, 661288.
154. Pei, L.; Yan, D.; He, Q.; Kong, J.; Yang, M.; Ruan, H.; Lin, Q.; Huang, L.; Huang, J.; Lin, T.; et al. LncRNA MIR4435-2HG Drives Cancer Progression by Modulating Cell Cycle Regulators and mTOR Signaling in Stroma-Enriched Subtypes of Urothelial Carcinoma of the Bladder. Cell. Oncol. 2023, 46, 1509–1527.
155. Dong, X.; Yang, Z.; Yang, H.; Li, D.; Qiu, X. Long Non-Coding RNA MIR4435-2HG Promotes Colorectal Cancer Proliferation and Metastasis Through miR-206/YAP1 Axis. Front. Oncol. 2020, 10, doi:10.3389/fonc.2020.00160.
156. Luo, P.; Wu, S.; Ji, K.; Yuan, X.; Li, H.; Chen, J.; Tian, Y.; Qiu, Y.; Zhong, X. LncRNA MIR4435-2HG Mediates Cisplatin Resistance in HCT116 Cells by Regulating Nrf2 and HO-1. PLoS One 2020, 15, doi:10.1371/journal.pone.0223035.
157. Bai, J.; Xu, J.; Zhao, J.; Zhang, R. Downregulation of lncRNA AWPPH Inhibits Colon Cancer Cell Proliferation by Downregulating GLUT-1. Oncol. Lett. 2019, 18, doi:10.3892/ol.2019.10515.
158. Lin, C.; Zhang, Y.; Chen, Y.; Bai, Y.; Zhang, Y. Retraction Note: Long Noncoding RNA LINC01234 Promotes Serine Hydroxymethyltransferase 2 Expression and Proliferation by Competitively Binding miR-642a-5p in Colon Cancer. Cell Death Dis. 2023, 14, 412.
159. Tang, C.; Li, C.; Chen, C.; Chen, T.; Zhu, J.; Sun, M.; Wang, P.; Han, C. LINC01234 Promoted Malignant Behaviors of Breast Cancer Cells via Hsa-miR-30c-2-3p/CCT4/mTOR Signaling Pathway. Taiwan. J. Obstet. Gynecol. 2024, 63, 46–56.
160. Liu, Z.; Ma, L.; Gu, Y.; Huang, Y.; Liang, X.; Kong, L.; Sun, Y. Long Non-Coding RNA LINC01123 Promotes Cell Proliferation, Migration and Invasion via Interacting with SRSF7 in Colorectal Cancer. Pathol. Res. Pract. 2022, 232, 153843.
161. Shang, T.; Pang, S.; Dong, Y. Knockdown of Long Non-Coding RNA LINC01123 Plays a Molecular Sponge on miR-625-5p to Inhibit the Process of Colorectal Cancer Cells via LASP1. J. Mol. Histol. 2023, 54, 521–537.
162. Statement of Retraction: STAT1-Induced Upregulation of lncRNA LINC01123 Predicts Poor Prognosis and Promotes the Progression of Endometrial Cancer through miR-516b/KIF4A. Cell Cycle 2023, 22, 1158.
163. Wang, H.; He, D. LINC01123 Acts as an Oncogenic Driver in Lung Adenocarcinoma by Regulating the miR-4766-5p/PYCR1 Axis. Histol. Histopathol. 2023, 38, 1475–1486.
164. Dong, B.; Li, C.; Xu, X.; Wang, Y.; Li, Y.; Li, X. LncRNA LINC01123 Promotes Malignancy of Ovarian Cancer by Targeting Hsa-miR-516b-5p/VEGFA. Genes Genomics 2024, 46, 231–239.
165. Wang, J.; Wu, M.; Chang, L.; Jin, Z.; Yang, X.; Li, D.; Wang, J.; Qu, J.; Hou, Q.; Huang, X.; et al. The lncRNA TERC Promotes Gastric Cancer Cell Proliferation, Migration, and Invasion by Sponging miR-423-5p to Regulate SOX12 Expression. Annals of Translational Medicine 2022, 10, doi:10.21037/atm-22-3545.

 doi:10.20944/preprints202403.0787.v1



166. Norouzi, R.; Mohamadzade, Z.; Norouzi, R.; Norouzi, R.; Esmaeili, R.; Soltani, B.M. In-Silico and in-Vitro Evidence Suggest LINC01405 as a Sponge for miR-29b and miR-497-5p, and a Potential Regulator of Wnt, PI3K, and TGFB Signaling Pathways in Breast Carcinoma. Cancer Rep. 2024, e1972.
167. Shi, L.; Magee, P.; Fassan, M.; Sahoo, S.; Leong, H.S.; Lee, D.; Sellers, R.; Brullé-Soumaré, L.; Cairo, S.; Monteverde, T.; et al. A KRAS-Responsive Long Non-Coding RNA Controls microRNA Processing. Nat. Commun. 2021, 12, 2038.
168. Yang, M.-H.; Zhao, L.; Wang, L.; Ou-Yang, W.; Hu, S.-S.; Li, W.-L.; Ai, M.-L.; Wang, Y.-Q.; Han, Y.; Li, T.-T.; et al. Nuclear lncRNA HOXD-AS1 Suppresses Colorectal Carcinoma Growth and Metastasis via Inhibiting HOXD3-Induced Integrin β3 Transcriptional Activating and MAPK/AKT Signalling. Mol. Cancer 2019, 18, 31.
169. Zhang, H.; Wang, Y.; Lu, J.; Zhao, Y. Long Non-Coding RNA LINC00222 Regulates GSK3β Activity and Promotes Cell Apoptosis in Lung Adenocarcinoma. Biomed. Pharmacother. 2018, 106, 755–762.
170. Tang, Y.; Ji, F. lncRNA HOTTIP Facilitates Osteosarcoma Cell Migration, Invasion and Epithelial-Mesenchymal Transition by Forming a Positive Feedback Loop with c-Myc. Oncol. Lett. 2019, 18, 1649–1656.